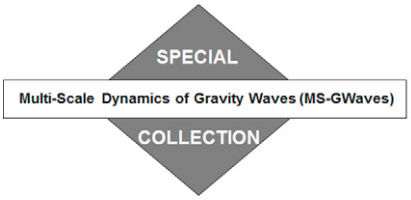

Three-Dimensional Static Instability of Gravity Waves and a Possible Parameterization of the Associated Wave Breaking

SEBASTIAN BORCHERT[a] AND GÜNTHER ZÄNGL[a]

[a] *Deutscher Wetterdienst, Offenbach, Germany*

(Manuscript received 26 October 2021, in final form 26 July 2022)

ABSTRACT: Parameterizations of subgrid-scale gravity waves (GWs) in atmospheric models commonly involve the description of the dissipation of GWs. Where they dissipate, GWs have an increased effect on the large-scale flow. Instabilities that trigger wave breaking are an important starting point for the route to dissipation. Possible destabilizing mechanisms are numerous, but the classical vertical static instability is still regarded as a key indicator for the disposition to wave breaking. In this work, we investigate how the horizontal variations associated with a GW could alter the criterion for static instability. To this end, we use an extension of the common parcel displacement method. This three-dimensional static stability analysis predicts a significantly larger range of instability than does the vertical static stability analysis. In this case, the Lindzen-type saturation adjustment to a state of marginal stability is perhaps a less suitable ansatz for the parameterization of the GW breaking. To develop a possible ansatz for the GW dissipation due to three-dimensional instability, we apply the methods of irreversible thermodynamics, which are embedded in the Gibbs formalism of dynamics. In this way, the parameterization does not only satisfy the second law of thermodynamics, but it can also be made consistent with the conservation of energy and further (non-)conservation principles. We develop the parameterization for a discrete spectrum of GW packets. Offline computations of GW drag and dissipative heating rates are performed for two vertical profiles of zonal wind and temperature for summer and winter conditions from CIRA data. The results are compared to benchmarks from the literature.

KEYWORDS: Gravity waves; Instability; Parameterization

1. Introduction

Internal gravity waves (GWs) are prominent dynamic structures that emerge in the atmosphere. If considered as separate physical entities, their life cycle may be divided into three stages. First, their forcing, which is frequently encountered in the troposphere due to processes such as the flow over uneven terrain, convection, and the spontaneous emission by synoptic-scale flow structures. Second, their propagation, which might lead them into upper layers of the atmosphere, where, third, different processes lead to an increased attenuation of GWs until they disappear. This last stage of their life cycle is associated with a drag exerted on the large-scale flow ("large scale" compared to the characteristic wavelength of the GWs), which makes this process relevant to the dynamics of the global circulations in the middle and upper atmosphere (Fritts and Alexander 2003; Kim et al. 2003).

Instabilities are believed to be an important trigger of GW attenuation and there is a vast number of possible mechanisms that are counted among them (Dunkerton 1989; Fritts 1989; Sonmor and Klaassen 1997; Fritts and Alexander 2003; Schlutow 2019). Two of the most thoroughly investigated mechanisms are probably the vertical static instability (VSI; also referred to as convective instability) and the vertical dynamic instability (VDI; e.g., Hodges 1967). The atmospheric state, modified by the presence of GWs, is commonly said to be dynamically or statically unstable, if its Richardson number satisfies $\mathrm{Ri} < 1/4$ or $\mathrm{Ri} < 0$, respectively. A process that almost inevitably leads to one of the aforementioned criteria being satisfied is the vertical propagation of GWs, since their amplitude tends to increase exponentially as the density decreases exponentially. Where the atmospheric state is unstable the GWs are likely to break. In the course of this process, turbulence develops and the larger-scale flow experiences a drag (e.g., Fritts and Alexander 2003).

Many methods to investigate the stability of an atmospheric state may either be classed among the wave-dynamical or the parcel-dynamical stability analyses. In the former class of analyses the atmospheric state, whose stability shall be analyzed, is expanded by wavelike perturbations. Nongrowing (growing) perturbation amplitudes indicate that the state is stable (unstable) with respect to perturbations of the prescribed wave characteristics. The other class of analyses, in contrast, deduces the stability of an atmospheric state at a particular point by investigating the evolution of a displaced air parcel. If it tends to diverge from the point, the state is

Corresponding author: Sebastian Borchert, sebastian.borchert@dwd.de

DOI: 10.1175/JAS-D-21-0287.1

classed as unstable there (Godson 1950). The VSI, for instance, is commonly identified by parcel-dynamical stability analyses, where the air parcels are displaced in vertical direction (e.g., Holton 2004; Zdunkowski and Bott 2004). As a hand-waving bridging between the two approaches, a displaced parcel could be thought of as delta-function-like perturbation, which in turn may be regarded as composed of an entire spectrum of wave perturbations, all having the same amplitude.

Nonhydrostatic GWs may be associated with significant horizontal gradients, if the vertical gradients are significant, too, since their horizontal and vertical wavelengths are comparable in size (Fritts and Alexander 2003; Kim et al. 2003). Hines (1971, 1988), for instance, investigated, if such horizontal gradients can influence the stability of a GW. He used a variant of the aforementioned parcel-dynamical stability analyses, where the interchange of two parcels, being located relatively close to each other on some specified axis, is considered. The criterion for instability is based on energetic aspects. Static instability is said to be present, if the interchange would result in a reduction of gravitational potential energy, and dynamic instability is made conditional on the reduction of potential energy outweighing the increase of kinetic energy by the interchange of the parcels. The axis on which the two parcels are located initially can have any orientation, so these types of instability are commonly termed slantwise static or dynamic instability (SSI or SDI, respectively; e.g., Marks and Eckermann 1995). Within the framework of this approach, the criteria for VSI and VDI are in a sense special cases of SSI and SDI for a vertically aligned axis. An important result of the SSI of GWs is that for certain regions in a wave train there is always a set of axes for which the criterion for instability is satisfied. So, in contrast to the predictions of VSI, GWs are always unstable, regardless of their amplitudes. If a GW passes through a point, the atmospheric state there changes periodically between being stable and unstable. Therefore, the mere magnitude of the instability is probably not enough to infer the strength of the wave breaking. If the wave period is short compared to the characteristic time scale associated with the instability, the formation of the wave breaking is periodically interrupted at the considered point (Hines 1988; Marks and Eckermann 1995).

The conditions for SSI and SDI depend on the direction of the axis on which the two parcels are located initially. This property might be unfavorable for applications, which only depend on the synopsis if the atmospheric state is unstable at some location or not. To eliminate the dependence on the direction, one can integrate over interchanges along all possible directions. This, however, introduces a number of additional assumptions that might appear more or less arbitrary. Hines (1971), for instance, considered a spherical volume, in which each parcel is interchanged with the parcel diametrically opposite. To avoid such complications, we present a possible alternative to the parcel interchange method, which is based on an extension of the classical vertical-displacement method. To analyze the atmospheric state for instability at some location, one considers the tendency of motion of the parcel there after it being displaced in an arbitrary direction. This results in an equation for the oscillation frequency of the parcel, which depends on the characteristics of the atmospheric state at the location, but does not depend on the displacement. Then imaginary oscillation frequencies (of a certain sign) are associated with an unstable state (Godson 1950; Shutts and Cullen 1987). We call the instability three-dimensional static instability (3DSI), since it can be regarded as an extension of VSI that takes into account the horizontal variation of the atmospheric state. A significant portion of GWs that are stable with respect to VSI, are unstable with respect to 3DSI. In that regard, 3DSI agrees with SSI.

It is common practice to parameterize the unresolved (or subgrid-scale) GWs in atmospheric models, whose characteristic spatial and temporal resolution scales exclude a significant part of the GW spectrum from being resolved. That is, those unresolved processes, which have a significant effect on the resolved flow, are modeled by some effective formulation that depends on properties of the resolved flow (e.g., Gardner 1996; McLandress 1998; Fritts and Alexander 2003; Kim et al. 2003; Medvedev and Yiğit 2019). Ideally, the integration of a GW parameterization into an atmospheric model would bring simulation results closer to the results from a model that resolves most of the GW spectrum or to observations (with respect to some specified quality measures). Here, we mainly focus on the parameterization of the process of GW breaking and the associated effects on the resolved atmospheric state. A common approach is the one introduced by Lindzen (1981), where the GW breaking is made conditional on a static instability. As a consequence of the breaking, the GWs are assumed to saturate to a state of marginal stability (e.g., Lindzen 1981; Warner and McIntyre 2001; Scinocca 2003) or to be obliterated completely (e.g., Alexander and Dunkerton 1999). This in turn leads to a convergence of momentum flux, which is the GW drag on the resolved flow. There are other approaches such as the Doppler-spread parameterization of Hines (1997). Which of the many parameterization approaches performs best with respect to certain quality measures, is still a matter of debate and active research (e.g., Gardner 1996; McLandress 1998; Fritts and Alexander 2003; McLandress and Scinocca 2005; Majdzadeh and Klaassen 2019, hereafter MK19; Plougonven et al. 2020).

The nonlinear process of GW breaking is commonly regarded as an irreversible process (e.g., Medvedev and Klaassen 2003; Shaw and Shepherd 2009; Gassmann and Herzog 2015; Gassmann 2018); therefore, the methods of irreversible thermodynamics (e.g., Herbert 1978; Jou et al. 2001; Zdunkowski and Bott 2003, 2004; Papenfuß 2020) may be a possible tool for the development of a parameterization, and we will use it in this work.

The paper is organized as follows. In section 2 we describe the stability analysis that underlies 3DSI, and apply it to a monochromatic GW in section 3. The ansatz for a parameterization of the effects that are associated with the 3DSI-induced breaking of subgrid-scale GWs can be found in section 4. For two vertical profiles of zonal wind and temperature, we show results for GW drag and dissipative heating rates in section 5, and conclude with a summary in section 6.

2. Parcel-dynamical stability analysis

In this section we describe the three-dimensional parcel stability analysis as set out by Godson (1950) and Shutts and Cullen (1987), for instance.[1] We start with the equation of motion of an air parcel (e.g., Holton 2004; Gassmann and Herzog 2015):

$$\frac{d^2\mathbf{x}}{dt^2} + 2\boldsymbol{\Omega} \times \frac{d\mathbf{x}}{dt} + \boldsymbol{\nabla}\Phi + c_p\theta\boldsymbol{\nabla}\pi = 0, \tag{1}$$

where d/dt denotes the Lagrangian time derivative, $\mathbf{x}$ stands for the position vector of the parcel, $\boldsymbol{\Omega}$ is the vector of Earth's angular velocity, Φ is the potential of apparent gravity (i.e., the potential of true gravity plus the potential of centrifugal acceleration), $\theta = T/\pi$ is the potential temperature, with temperature T and Exner pressure $\pi = (p/p_{00})^{R/c_p}$, where p is the pressure and p_{00} is a reference pressure (e.g., $p_{00} = 1000$ hPa). In addition, c_p and R denote the specific heat capacity at constant pressure and the gas constant of dry air, respectively. Finally, $\boldsymbol{\nabla}$ stands for the gradient. A list of frequently used symbols can be found in appendix D. The model includes reversible processes. Irreversible processes, such as viscous momentum fluxes are ignored. In addition, the model is restricted to dry air. To simplify the following calculations, we write the Coriolis acceleration in the following form (cf. Wilson 1929; Zdunkowski and Bott 2003):

$$2\boldsymbol{\Omega} \times \mathbf{v} = 2\boldsymbol{\Omega} \times (\mathbf{I} \cdot \mathbf{v}) = 2(\boldsymbol{\Omega} \times \mathbf{I}) \cdot \mathbf{v} = 2\mathbf{W} \cdot \mathbf{v}, \tag{2}$$

where $\mathbf{v} = d\mathbf{x}/dt$ is the parcel's velocity, $\mathbf{I}$ denotes the second-order identity tensor, and we call $\mathbf{W} := \boldsymbol{\Omega} \times \mathbf{I}$ the (second-order) angular velocity tensor. This tensor is constant and antisymmetric, i.e., $\mathbf{W}^{\mathrm{T}} = -\mathbf{W}$, where T denotes the transpose. The second step in Eq. (2) makes use of $(\mathbf{a} \times \mathbf{A}) \cdot \mathbf{b} = \mathbf{a} \times (\mathbf{A} \cdot \mathbf{b}) = \mathbf{a} \times \mathbf{A} \cdot \mathbf{b}$, which holds for arbitrary vectors $\mathbf{a}$ and $\mathbf{b}$ and an arbitrary tensor $\mathbf{A}$ (e.g., Wilson 1929). Now, for the purpose of the stability analysis the air parcel is virtually displaced from its current position $\mathbf{x}$ to the position $\mathbf{X}$. Here, "virtual" means basically that the process, which might lead to such displacement remains unspecified. The displacement shall take place quasi instantaneously, so that temporal changes of field quantities during the displacement can be neglected. In addition, the environment shall remain quasi unaffected. Clearly, these are highly idealized conditions and this has to be kept in mind when interpreting the results of the stability analysis. Following the displacement, the parcel again moves according to the equation of motion. Therefore, the evolution of the distance between the perturbed parcel and the parcel if it would have remained unperturbed is given by (Godson 1950; Shutts and Cullen 1987)

$$\frac{d^2\delta\mathbf{x}}{dt^2} + 2\mathbf{W} \cdot \frac{d\delta\mathbf{x}}{dt} + \delta(\boldsymbol{\nabla}\Phi) + c_p\delta(\theta\boldsymbol{\nabla}\pi) = 0. \tag{3}$$

Here, δ denotes the difference of a quantity between the positions $\mathbf{X}$ and $\mathbf{x}$. For instance, $\delta\mathbf{x} := \mathbf{X} - \mathbf{x}$ and $\delta(\boldsymbol{\nabla}\Phi) := \boldsymbol{\nabla}\Phi|_{\mathbf{X}} - \boldsymbol{\nabla}\Phi|_{\mathbf{x}}$. We assume that the length of the distance $\delta\mathbf{x}$ is sufficiently small for a spatial Taylor expansion to first order to provide a relatively good approximation $\delta(\boldsymbol{\nabla}\Phi) \approx \delta\mathbf{x} \cdot \boldsymbol{\nabla}\boldsymbol{\nabla}\Phi|_{\mathbf{x}}$, with the Hessian $\boldsymbol{\nabla}\boldsymbol{\nabla}$. The subscript $\mathbf{x}$ will be omitted in the following. The fourth term on the lhs of Eq. (3) can be approximated by $c_p\delta(\theta\boldsymbol{\nabla}\pi) \approx c_p[(\delta\theta)\boldsymbol{\nabla}\pi + \theta\delta(\boldsymbol{\nabla}\pi)] \approx c_p[(\delta\theta)\boldsymbol{\nabla}\pi + \theta\delta\mathbf{x} \cdot \boldsymbol{\nabla}\boldsymbol{\nabla}\pi]$. In addition, we assume that the displacement is an adiabatic change of state, so $\delta\theta = 0$. This yields for Eq. (3) (cf. Godson 1950; Shutts and Cullen 1987)

$$\left[\mathbf{I}\frac{d^2}{dt^2} + 2\mathbf{W}\frac{d}{dt} + \underbrace{(\boldsymbol{\nabla}\boldsymbol{\nabla}\Phi + c_p\theta\boldsymbol{\nabla}\boldsymbol{\nabla}\pi)_{\mathbf{x},t=0}}_{=:\mathbf{S}}\right] \cdot \delta\mathbf{x} = 0, \tag{4}$$

where $\mathbf{S}$ is referred to as the stability tensor.[2] We used the symmetry of the Hessian when making $\delta\mathbf{x}$ the second factor in all terms [e.g., $\delta\mathbf{x} \cdot \boldsymbol{\nabla}\boldsymbol{\nabla}\Phi = (\boldsymbol{\nabla}\boldsymbol{\nabla}\Phi)^{\mathrm{T}} \cdot \delta\mathbf{x} = \boldsymbol{\nabla}\boldsymbol{\nabla}\Phi \cdot \delta\mathbf{x}$]. Since all summands of $\mathbf{S}$ are symmetric, $\mathbf{S}$ is symmetric, too. The evaluation of the stability tensor takes place at the position of the unperturbed parcel $\mathbf{x}$ and at the time of the displacement $t = 0$. The latter restriction is not necessary, in principle, as long as the distance between the perturbed and unperturbed parcel remains small, and as long as diabatic processes are relatively weak. However, using $\mathbf{S}|_{t=0} = \text{const.}$ simplifies solving Eq. (4) analytically. As long as any typical time scale that can be assigned to Eq. (4) is small as compared to the time scale of the atmospheric flow, whose stability is investigated, this restriction is acceptable. In the following, we will omit the subscripts $\mathbf{x}, t = 0$.

The linear second-order differential equation (4) is the basis of the stability analysis. As an example of application, we consider the vertical displacement of a parcel in a horizontally homogeneous atmosphere on the f plane. In this case, Eq. (4) reduces to

$$\frac{d^2\delta z}{dt^2} + \underbrace{\left(c_p\theta\frac{\partial^2\pi}{\partial z^2}\right)}_{=:\overline{N}^2}\delta z = 0. \tag{5}$$

Here, z denotes the vertical coordinate and we refer to $\overline{N}^2$ as the squared buoyancy frequency. Under the f-plane approximation, there are no contributions of the Coriolis acceleration and of $\boldsymbol{\nabla}\boldsymbol{\nabla}\Phi$ to Eq. (5). The latter, because $\boldsymbol{\nabla}\Phi = \mathbf{g} = g\mathbf{e}_z = \text{const.}$ holds on the f plane, where g is the mean gravitational acceleration at sea level and $\mathbf{e}_z$ is the vertical unit vector. Equation (5) is the common buoyancy oscillation equation and forms one possible starting point for the investigation of static stability (e.g., Holton 2004). There is a slight difference as compared to the standard equation, where the squared Brunt–Väisälä frequency

$$N^2 := \frac{g}{\theta}\frac{\partial\theta}{\partial z}, \tag{6}$$

[1] In fact, we closely follow the work of Ertel et al. (1941) in a large part of the parcel stability analysis, but no English translation is available, as far as we know.

[2] Expressed in terms of pressure p and density ρ, the stability tensor reads $\mathbf{S} = \boldsymbol{\nabla}\boldsymbol{\nabla}\Phi + \rho^{-1}[\boldsymbol{\nabla}\boldsymbol{\nabla}p - (c_v/c_p/p)(\boldsymbol{\nabla}p)(\boldsymbol{\nabla}p)]$ (see Ertel et al. 1941).

in place of $\overline{N}^2$, is the factor in front of δz. The relation between the two is as follows: if we assume that the vicinity of the displaced parcel is in hydrostatic balance, it follows from Eq. (1) that $\partial\pi_0/\partial z = -g/c_p/\theta_0$, where the subscript 0 denotes hydrostatic balance. With this, we find that the values of both frequencies coincide under hydrostatic conditions:

$$\overline{N}_0^2 = c_p\theta_0\frac{\partial}{\partial z}\left(-\frac{g}{c_p\theta_0}\right) = \frac{g}{\theta_0}\frac{\partial\theta_0}{\partial z} = N_0^2. \tag{7}$$

The general equation (4) may be written as $\mathbf{D}\cdot\delta\mathbf{x} = 0$, where $\mathbf{D}$ denotes the linear tensor operator with constant tensor coefficients. Multiplying the adjugate tensor operator adj($\mathbf{D}$) yields adj($\mathbf{D}$) $\cdot\ \mathbf{D}\cdot\delta\mathbf{x} = \det(\mathbf{D})\mathbf{I}\cdot\delta\mathbf{x} = \det(\mathbf{D})\delta\mathbf{x} = 0$, where det($\mathbf{D}$) is the determinant of $\mathbf{D}$. This form of the equation is sufficient for our purposes; for Eq. (4) it reads (compare, e.g., Bronshtein et al. 1990)

$$\left(\frac{d^6}{dt^6} + a\frac{d^4}{dt^4} + b\frac{d^2}{dt^2} + c\right)\delta\mathbf{x} = 0. \tag{8}$$

The detailed expressions of the scalar coefficients a, b, and c can be found in appendix A. Now, we consider a parcel distance evolving according to $\delta\mathbf{x} = \delta\hat{\mathbf{x}}e^{-i\overline{\omega}t}$, with the imaginary unit i and constant complex amplitude $\delta\hat{\mathbf{x}}$ and oscillation frequency $\overline{\omega}$. If we insert this ansatz in Eq. (8) and multiply by (-1), we find the characteristic equation (cf. Godson 1950; Shutts and Cullen 1987; Bronshtein et al. 1990):

$$(\overline{\omega}^2)^3 - a(\overline{\omega}^2)^2 + b(\overline{\omega}^2) - c = 0. \tag{9}$$

This cubic equation in $\overline{\omega}^2$ is, for our purposes, the central result of the parcel stability analysis. If one of its roots $\overline{\omega}_j^2$, $j = 1$, 2, 3, satisfies $\overline{\omega}_j^2 < 0$, the distance between the perturbed and unperturbed parcel tends to increase exponentially. This, in turn, means that the atmospheric state in the vicinity of the parcel is unstable, at least as far as this stability analysis is concerned.

3. Application to a GW

We consider an atmospheric state, which varies relatively slowly in space and time and is modified by a single monochromatic plane nonhydrostatic GW, and analyze the stability of this state with the characteristic Eq. (9). To simplify the problem, we make a number of assumptions. First, we consider the atmospheric state on an f plane and write for the fields of the potential temperature and the Exner pressure (cf. Achatz et al. 2017):

$$\psi(\mathbf{x},t) = \psi_0(\mathbf{x},t) + \psi'(\mathbf{x},t) = \psi_0(\mathbf{x},t) + \mathrm{Re}\{\hat{\psi}(\mathbf{x},t)e^{i\varphi}\}, \tag{10}$$

with $\psi = \theta, \pi$. Here $(\cdot)_0$ denotes the atmospheric background state and $(\cdot)'$ stands for the perturbation associated with the GW. In addition, Re denotes the real part, $\widehat{(\cdot)}$ is the wave amplitude, and $\varphi = \mathbf{k}\cdot\mathbf{x} - \omega t$ is the wave phase, with wave vector $\mathbf{k}$ and extrinsic frequency ω. The wave amplitude is assumed to vary on longer spatial and temporal scales than the wave phase φ. As a further approximation, we assume that the horizontal variation of the atmospheric state is dominated by the GW, i.e.,

$$\left|\frac{\partial^2\pi_0}{\partial x_i\partial x_j}\right| \ll \left|\frac{\partial^2\pi'}{\partial x_i\partial x_j}\right|, \tag{11}$$

with $x_i, x_j \in \{x, y, z\}$ (x, y, and z being the zonal, meridional, and vertical coordinates, respectively), except for the vertical variation:

$$\left|\frac{\partial^2\pi_0}{\partial z^2}\right| \gtrless \left|\frac{\partial^2\pi'}{\partial z^2}\right|. \tag{12}$$

Therefore, we may approximate the stability tensor in Eq. (4) by

$$\begin{aligned}\mathbf{S} &= c_p\theta\boldsymbol{\nabla}\boldsymbol{\nabla}\pi \approx c_p(\theta_0+\theta')\left(\mathbf{e}_z\mathbf{e}_z\frac{\partial^2\pi_0}{\partial z^2} + \boldsymbol{\nabla}\boldsymbol{\nabla}\pi'\right)\\ &= \overline{N}^2\left(1+\frac{\theta'}{\theta_0}\right)\left[\mathbf{e}_z\mathbf{e}_z + \left(\frac{\partial^2\pi_0}{\partial z^2}\right)^{-1}\boldsymbol{\nabla}\boldsymbol{\nabla}\pi'\right]\\ &= \overline{N}^2\left[\mathbf{e}_z\mathbf{e}_z + \left(\frac{\partial^2\pi_0}{\partial z^2}\right)^{-1}\boldsymbol{\nabla}\boldsymbol{\nabla}\pi' + \frac{\theta'}{\theta_0}\mathbf{e}_z\mathbf{e}_z + \left(\frac{\partial^2\pi_0}{\partial z^2}\right)^{-1}\frac{\theta'}{\theta_0}\boldsymbol{\nabla}\boldsymbol{\nabla}\pi'\right].\end{aligned} \tag{13}$$

The dispersion relation of GWs under the Boussinesq approximation reads (e.g., Fritts and Alexander 2003; Muraschko et al. 2015; Achatz et al. 2017)

$$\hat{\omega}^2 = (\omega - \mathbf{k}\cdot\mathbf{v}_0)^2 = \frac{\mathbf{k}\cdot\mathbf{N}^2\cdot\mathbf{k}}{\mathbf{k}\cdot\mathbf{k}} = \frac{N^2(k_x^2+k_y^2) + f^2k_z^2}{k_x^2+k_y^2+k_z^2}, \tag{14}$$

where $\hat{\omega}$ is the intrinsic frequency, with $0 < \hat{\omega}^2 < N^2$, $\mathbf{v}_0$ is the wind vector of the background atmosphere, and k_x, k_y, and k_z are the zonal, meridional, and vertical components of the wave vector $\mathbf{k}$. In addition, the tensor $\mathbf{N}^2$ can be expanded according to $\mathbf{N}^2 = N^2(\mathbf{e}_x\mathbf{e}_x + \mathbf{e}_y\mathbf{e}_y) + f^2\mathbf{e}_z\mathbf{e}_z$ on the f plane, where $\mathbf{e}_x$ and $\mathbf{e}_y$ denote unit vectors in zonal and meridional directions, respectively. Given the Boussinesq approximation, we may neglect the spatial and temporal variations of the GW amplitude, i.e., $\hat{\theta}(\mathbf{x},t) \approx \hat{\theta} = \text{const.}$ and $\hat{\pi}(\mathbf{x},t) \approx \hat{\pi} = \text{const.}$ (e.g., Muraschko et al. 2015; Achatz et al. 2017). To simplify the expression (13), we compare the magnitudes of the four terms on the rhs. First, we neglect the fourth term, quadratic in the primed quantities, as we assume that its magnitude is small as compared to the magnitude of the other terms. We keep the second term on the rhs of Eq. (13) in unmodified form, because of the relation (12), and because we assume that horizontal variations of π' can significantly modify the static stability only if their magnitude and the magnitude of the vertical variations are similar in size. Finally, to estimate the third term on the rhs, we use that according to the polarization relations of GWs, the amplitude $\hat{\theta}$ may be expressed in terms of $\hat{\pi}$ (cf. Muraschko et al. 2015; Bölöni et al. 2016; Achatz et al. 2017):

$$\hat{\theta} = i\left(\frac{N^2}{N^2-\hat{\omega}^2}\right)\frac{c_p\theta_0^2}{g}k_z\hat{\pi} = i\frac{k^2}{k_z^2}\frac{c_p\theta_0^2}{g}k_z\hat{\pi}, \tag{15}$$

where we used Eq. (14) and $k^2 = \mathbf{k}\cdot\mathbf{k} = k_x^2 + k_y^2 + k_z^2$. While not required, we consider a specific wave amplitude, the amplitude at the point of neutral vertical static stability, which yields a rough estimate for the upper bound of the magnitude, as GWs with larger magnitudes might break. The result will also be useful below. At the point of neutral stability, the component $S_{zz} := \mathbf{e}_z\mathbf{e}_z \cdot\cdot\, \mathbf{S}$ [see Eqs. (A1) and (A6) in appendix A] vanishes. The factor $(1 + \theta'/\theta_0)$ on the rhs of Eq. (13) is nonzero as $\theta > 0$. This means

$$1 + \left(\frac{\partial^2\pi_0}{\partial z^2}\right)^{-1}\frac{\partial^2\pi'}{\partial z^2} = 1 + \frac{c_p\theta_0}{\overline{N}^2}\frac{\partial^2\pi'}{\partial z^2} = 0, \tag{16}$$

where we used that $\mathbf{e}_z\mathbf{e}_z \cdot\cdot\, \mathbf{e}_z\mathbf{e}_z = 1$ and $\mathbf{e}_z\mathbf{e}_z \cdot\cdot\, \boldsymbol{\nabla}\boldsymbol{\nabla}\pi' = \partial^2\pi'/\partial z^2$. Inserting the wave ansatz for π' from Eq. (10) yields $1 - (c_p\theta_0/\overline{N}^2)k_z^2\mathrm{Re}\{\hat{\pi}e^{i\varphi}\} = 0$, and for the least stable regions of a GW, we may write $1 - (c_p\theta_0/\overline{N}^2)k_z^2|\hat{\pi}| = 0$, where $|\cdot|$ denotes the modulus. This yields (cf. Hodges 1967; Hines 1988; Bölöni et al. 2016; Achatz et al. 2017)

$$|\hat{\pi}|_n = \frac{\overline{N}^2}{c_p\theta_0 k_z^2}, \tag{17}$$

$$\left|\frac{\theta'/\theta_0}{(c_p\theta_0/\overline{N}^2)\partial^2\pi'/\partial z^2}\right|_n = \frac{|\hat{\theta}|_n}{\theta_0} = \frac{k^2}{k_z^2}\frac{\overline{N}^2}{g|k_z|} = \left(1 + \frac{\lambda_z^2}{\lambda_h^2}\right)\frac{\lambda_z}{L_z}, \tag{18}$$

where the subscript n denotes the neutral point. We used Eq. (15) for the expression (18), and we introduced horizontal and vertical wavelengths $\lambda_h = 2\pi/\sqrt{k_x^2 + k_y^2}$ and $\lambda_z = 2\pi/|k_z|$ (here $\pi = 3.14159\ldots$), and length scale $L_z := 2\pi g/\overline{N}^2 \approx 200\,\mathrm{km}$ for the gravitational acceleration $g = 9.81\ \mathrm{m\ s^{-2}}$ and $\overline{N}^2 = 3.2\times10^{-4}\,\mathrm{s^{-2}}$. If we assume that $\lambda_h \gtrsim \lambda_z$ and $\lambda_z \lesssim 10\,\mathrm{km}$, $|\hat{\theta}|_n/\theta_0 \ll 1$ should hold. Therefore, we assume that the magnitude of the third term on the rhs of Eq. (13) is significantly smaller than the magnitudes of the first and second terms. Altogether, this supports the following approximation of the expression (13):[3]

$$\mathbf{S} \approx \underbrace{\overline{N}^2\mathbf{e}_z\mathbf{e}_z}_{=:\mathbf{S}_0} + \underbrace{c_p\theta_0\boldsymbol{\nabla}\boldsymbol{\nabla}\pi'}_{=:\mathbf{S}'}. \tag{19}$$

Inserting the wave ansatz for π' and focusing on the least stable region of the GW motivates the final expression for $\mathbf{S}'$, which we use henceforth:

$$\mathbf{S}' \approx -\mathbf{k}\mathbf{k}c_p\theta_0|\hat{\pi}|. \tag{20}$$

With Eq. (20), the coefficients a, b, and c of the characteristic Eq. (9) read [see Eqs. (A5) and (A8) in appendix A]

$$a = \overline{N}^2 - c_p\theta_0|\hat{\pi}|k^2 + f^2, \tag{21a}$$

$$b = -c_p\theta_0\overline{N}^2|\hat{\pi}|k_h^2 + f^2(\overline{N}^2 - c_p\theta_0|\hat{\pi}|k_z^2) \approx -c_p\theta_0\hat{\omega}^2k^2 + f^2\overline{N}^2, \tag{21b}$$

$$c = 0, \tag{21c}$$

with $k_h^2 = \mathbf{k}_h\cdot\mathbf{k}_h = k_x^2 + k_y^2$, where $\mathbf{k}_h$ is the horizontal part of the wave vector $\mathbf{k}$. We used $\overline{N}^2 \approx N^2$[see Eq. (7)] and the dispersion relation (14) in Eq. (21b). The respective solutions for the squared parcel oscillation frequencies are

$$(\overline{\omega}^2)_1 = 0, \tag{22a}$$

$$(\overline{\omega}^2)_{2,3} = \frac{\overline{N}^2 + f^2}{2}\times\left[1 - \eta k^2 \pm \sqrt{(1-\eta k^2)^2 + 4\eta k^2\frac{\hat{\omega}^2}{\overline{N}^2 + f^2} - \frac{4f^2\overline{N}^2}{(\overline{N}^2 + f^2)^2}}\right], \tag{22b}$$

with $\eta := c_p\theta_0|\hat{\pi}|/(\overline{N}^2 + f^2)$. In doing so, we assume that $\overline{N}^2 > 0$. The positive (negative) sign in front of the root sign on the rhs of Eq. (22b) belongs to $(\overline{\omega}^2)_2$ $[(\overline{\omega}^2)_3]$.

A nonvanishing coefficient c requires the Exner pressure π to vary in all three directions of an arbitrary normal basis [see Eq. (A8c) in appendix A]. In the case of a single monochromatic plane GW, however, there is variation in $\mathbf{e}_z$ and $\mathbf{k}$ directions only. For this reason, c vanishes in Eq. (21c). If two or more GWs interfere, with wave vectors pointing in different directions, we find $c \neq 0$, in general. This, in turn, affects all roots, where $(\overline{\omega}^2)_1 \neq 0$ could bring another type of instability into play.

We plotted solutions (22b), normalized by $(\overline{N}^2 + f^2)$ in Fig. 1. For that, we assumed an isothermal hydrostatically balanced background atmosphere, with a temperature of $T_0 = 300\,\mathrm{K}$ and a surface pressure of $p_s = 1013.25\,\mathrm{hPa}$. With the above value for g and $c_p = 1004.64\ \mathrm{J\ kg^{-1}\ K^{-1}}$ and $R = 287.04\ \mathrm{J\ kg^{-1}\ K^{-1}}$ this yields a scale height of $H = 8.8\,\mathrm{km}$ and $\overline{N}^2 = 3.2\times10^{-4}\,\mathrm{s^{-2}}$. We use $f^2 = f^2\,(\mathrm{lat} = 45°\mathrm{N}) \approx 10^{-8}\,\mathrm{s^{-2}}$ for the squared Coriolis parameter (see Holton 2004). Furthermore, we consider GWs at an altitude of $z = 50\,\mathrm{km}$, which yields $\theta_0 = 1522\,\mathrm{K}$. Finally, with $|\hat{\pi}| = |\hat{\pi}|_n(\lambda_z = 1.94\,\mathrm{km}) = 2\times10^{-5}$[see Eq. (17)] we obtain $\eta = 0.1\,\mathrm{km^2}$. In addition, we plotted the normalized squared oscillation frequency of the common vertical static stability analysis, which follows from assuming that each Cartesian component of the stability tensor (20), except for S_{zz}, vanishes:

$$\frac{(\overline{\omega}^2)_z}{\overline{N}^2} = 1 - \eta^* k_z^2, \tag{23}$$

with $\eta^* := c_p\theta_0|\hat{\pi}|/\overline{N}^2$. As can be shown from Eq. (22b), $(\overline{\omega}^2)_2 > 0$ and $(\overline{\omega}^2)_3 < 0$ would hold for $f^2 = 0$, since $k_h^2, k_z^2 > 0$. Therefore, the roots of $(\overline{\omega}^2)_3$ are imaginary and a displaced parcel tends to diverge from its original position. In the case of $f^2 = 0$, a GW is thus virtually always (marginally) unstable, as far as the three-dimensional static stability analysis on the approximation

[3] As an alternative to this approximation, the factor $\kappa := (1 + \theta'/\theta_0)$, with $0 < \kappa < 2$, could be absorbed into $\hat{\omega}^2$. Defining $\mathbf{S}_\star := \kappa^{-1}\mathbf{S}$, the coefficients of the characteristic Eq. (9) may be written $a = \kappa a_\star$, $b = \kappa^2 b_\star$ and $c = \kappa^3 c_\star$. Then $\kappa^{-3}\times$ [Eq. (9)] yields the transformed equation $(\overline{\omega}_\star^2)^3 - a_\star(\overline{\omega}_\star^2)^2 + b_\star(\overline{\omega}_\star^2) - c_\star = 0$, with $\overline{\omega}_\star^2 := \kappa^{-1}\overline{\omega}^2$. According to the polarization relation (15) there is a phase shift of $\pi/2$ between π' and θ'. At the wave crests and troughs of π', θ' is close to zero and $\kappa \approx 1$.

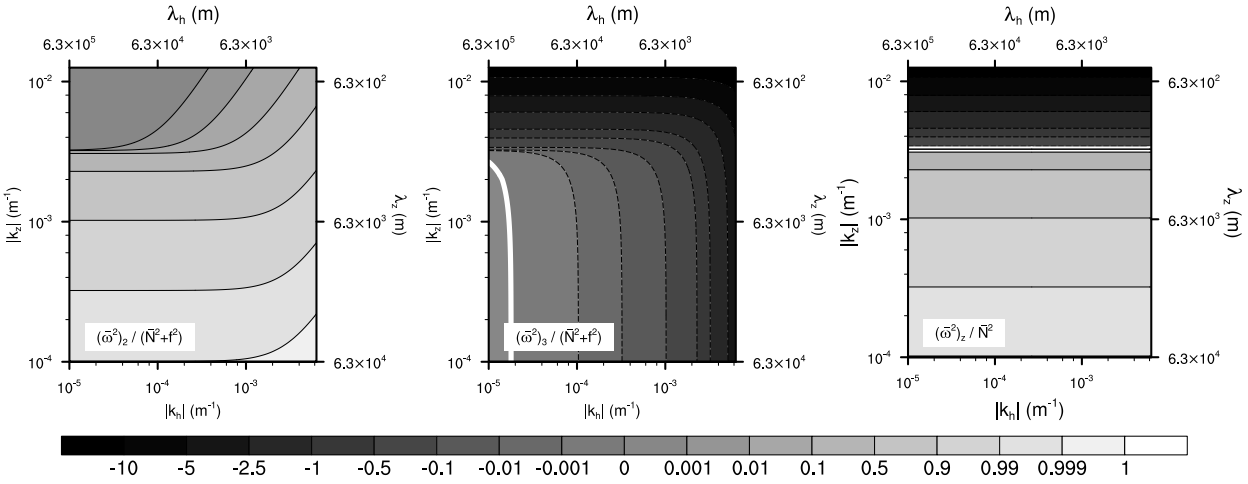

FIG. 1. (left),(center) Normalized second and third roots, $(\overline{\omega}^2)_2/(\overline{N}^2 + f^2)$ and $(\overline{\omega}^2)_3/(\overline{N}^2 + f^2)$, respectively, of the characteristic Eq. (9) [see Eq. (22b)]. (right) Normalized second root $(\overline{\omega}^2)_z/\overline{N}^2$ for the case that each Cartesian component of the stability tensor (20) vanishes, except for the component S_{zz} [see Eq. (23)]. The bottom x axis and left y axis show magnitudes of the horizontal and the vertical wavenumbers $|k_h|$ and $|k_z|$ in m^{-1}, respectively. The top x axis and right y axis show the corresponding horizontal and vertical wavelengths λ_h and λ_z in m. Solid contour lines indicate positive; dashed lines indicate negative values. The thick white line is the zero contour (see center and right panels). Negative values are associated with unstable conditions. See text for further parameters.

(20) is concerned. This changes if $f^2 \neq 0$, because of the negative sign of the third term of the radicand in Eq. (22b). For relatively small values of η (i.e., small wave amplitudes $|\hat{\pi}|$) and relatively large horizontal and vertical wavelengths, the root $(\overline{\omega}^2)_3$ may become positive (see Fig. 1, bottom-left corner of the plot shown in the middle panel). Under even more extreme conditions, the roots $(\overline{\omega}^2)_{2,3}$ may become complex. Nevertheless, if we compare the middle and right panels of Fig. 1, we see that the three-dimensional static stability analysis classifies a significantly larger area of the wavenumber space (referred to as **k** space in the following) as unstable than does the vertical static stability analysis. Where $(\overline{\omega}^2)_z/\overline{N}^2 < 0$, the values of $(\overline{\omega}^2)_z/\overline{N}^2$ and $(\overline{\omega}^2)_3/(\overline{N}^2 + f^2)$ approach each other with decreasing vertical wavelength. The main difference between the two lies in their dependence on the horizontal wavelength. While $(\overline{\omega}^2)_z$ does not depend on k_h^2, $(\overline{\omega}^2)_3$ decreases with decreasing horizontal wavelength. In summary, the more nonhydrostatic the GW the stronger the potential instability predicted by the three-dimensional static stability analysis, and the more the predictions of the three-dimensional and vertical stability analyses differ from each other.

In section 2, we mentioned that the parcel-dynamical stability analysis depends on a scale separation between the time scale of the atmospheric flow, whose stability is investigated, on the one hand, and the time scale of the motion of the displaced parcel, on the other hand. If we assume that the typical time scale of the GW is determined by its intrinsic frequency, we may assess the scale separation by the ratio

$$\tau := H[-(\overline{\omega}^2)_3]\left|\frac{(\overline{\omega}^2)_3}{\hat{\omega}^2}\right|^{1/2} = H[-(\overline{\omega}^2)_3]\frac{\mathcal{T}_{\mathrm{GW}}}{\mathcal{T}_{\mathrm{in}}}, \qquad (24)$$

where $\mathcal{T}_{\mathrm{in}} := 2\pi/|(\overline{\omega}^2)_3|^{1/2}$ denotes the time scale associated with the motion of the displaced parcel, referred to as instability time scale for $(\overline{\omega}^2)_3 < 0$, and $\mathcal{T}_{\mathrm{GW}} := 2\pi/|\hat{\omega}^2|^{1/2}$ is the GW time scale. In addition, $H(\cdot)$ stands for the Heaviside step function, which is equal to one for arguments >0 and equal to zero elsewhere (cf. Bronshtein et al. 1990). This ratio is shown in Fig. 2. The parameters are the same as for Fig. 1. We assume that the time scale separation is satisfied where $\tau \gg 1$. In this area of the **k** space, there is probably sufficient time for an instability to develop. Where $\tau \lesssim 1$, however, the periodic motion of the GW can obstruct the development.

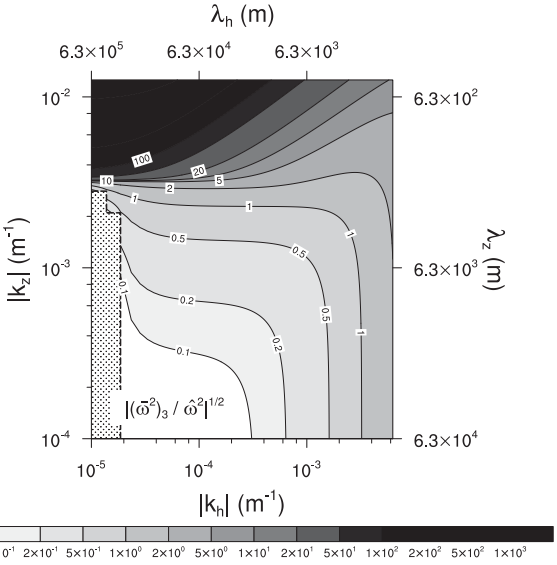

FIG. 2. Ratio of the instability times scale to the GW time scale, $\mathcal{T}_{\mathrm{GW}}/\mathcal{T}_{\mathrm{in}}$ [see Eq. (24)]. The same parameters are used as for Fig. 1. The dotted region in the bottom-left corner of the plot is stable, as $(\overline{\omega}^2)_3 > 0$ holds there (cf. Fig. 1, center).

Note that both Figs. 1 and 2 show the situation for a specific wave amplitude (here, $|\hat{\pi}| = 2 \times 10^{-5}$). In general, an increase of the wave amplitude leads to an expansion of the unstable area in **k** space. If we take a wave vector **k** that is unstable, the magnitude $|(\overline{\omega}^2)_3|$ increases with increasing wave amplitude. At the same time, the instability time scale shrinks and the ratio (24) increases.

In summary, the three-dimensional stability analysis predicts instability for a significantly larger area in **k** space than does the vertical stability analysis. There is no significant horizontal stratification in the atmosphere, which could counteract destabilizing gradients associated with GWs (e.g., Sonmor and Klaassen 1997). The differences between the predictions of the two stability analyses may be particularly relevant to nonhydrostatic GWs, whose horizontal and vertical wavelengths are of comparable scale (Kim et al. 2003). We emphasize that the above results depend on the assumptions on which the parcel-dynamical stability analysis is based. Another stability model, which is founded on different assumptions, may come to more or less different conclusions. Nevertheless, the above findings are generally in line with the results of the slantwise static stability analysis of Hines (1971, 1988). The author also found that the condition for vertical static instability $[(\overline{\omega}^2)_z/\overline{N}^2 < 0]$ may be too restrictive in general. The condition for slantwise static instability is virtually always satisfied in some region of a GW.

4. Parameterization of GW breaking due to 3DSI

Approaches to the parameterization problem may be based on decomposing the atmospheric state into a resolved (or gridscale) part and unresolved (or subgrid-scale) deviations. This may be written $\psi = \psi_0 + \psi'$ for some state variable ψ, where the subscript 0 and the prime indicate resolved and unresolved parts, respectively. The Reynolds average, which we denote by the angle brackets $\langle\rangle$ here, is one possible operator for achieving the decomposition. By definition, $\langle\psi_0\rangle = \psi_0 = \langle\psi\rangle$ and $\langle\psi'\rangle = 0$ hold true (e.g., Holton 2004; Gassmann and Herzog 2015). This tool may be used in a number of ways. One option is to average the budget equations for momentum, heat, etc., which results in additional terms that are quadratic in the primed quantities. These terms typically arise from the advective transport, such as the Reynolds stress in case of the averaged momentum budget. If we assume that the deviations are due to unresolved GWs, we may insert the wave ansatz of Eq. (10). Combined with the polarization relations of GWs and an ansatz for the wave breaking (for instance, by a suitable imaginary part of the frequency ω), we may finally arrive at a parameterization for the contribution of the unresolved GWs to the averaged budget equations (cf. Becker and Schmitz 2002; Medvedev and Klaassen 2003; Becker 2004; Akmaev 2007).

Another way of using the decomposition, which we employ in this work, puts somewhat more emphasis on the concept of interacting systems. These are the subsystem *resolved atmosphere* on the one hand and the subsystem GW, to which we attribute the deviations, on the other hand. The starting point is the *fundamental relation* between the extensive quantities contained by a volume of air. This relation characterizes the considered system. If the relation can be solved explicitly for the energy E, we may write $E = \mathfrak{E}(\Psi_1, \Psi_2, \ldots, \Psi_m)$, where Ψ_i denote the other extensive quantities (such as mass, momentum, heat, and volume; see Herbert 1978; Jou et al. 2001; Zdunkowski and Bott 2004; Job and Herrmann 2006). The differential of the fundamental relation is usually referred to as the Gibbs equation (see section 4b below). Inserting the decomposition and collecting terms up to second order in the primed quantities yields

$$E \approx \mathfrak{E}(\Psi_{1,0}, \ldots, \Psi_{m,0}) + \sum_{i=1}^{m} \Psi_i' \frac{\partial \mathfrak{E}}{\partial \Psi_i}\bigg|_0 + \frac{1}{2} \sum_{i,j=1}^{m} \Psi_i' \Psi_j' \frac{\partial^2 \mathfrak{E}}{\partial \Psi_i \partial \Psi_j}\bigg|_0. \tag{25}$$

Its Reynolds average reads (cf. Herbert and Kucharski 1998)

$$\begin{aligned}\langle E \rangle &\approx \mathfrak{E}(\Psi_{1,0}, \ldots, \Psi_{m,0}) + \frac{1}{2} \sum_{i,j=1}^{m} \langle \Psi_i' \Psi_j' \rangle \frac{\partial^2 \mathfrak{E}}{\partial \Psi_i \partial \Psi_j}\bigg|_0 \\ &= \mathfrak{E}(\Psi_{1,0}, \ldots, \Psi_{m,0}) + \mathfrak{E}'(\Psi_{1,0}, \ldots, \Psi_{m,0}, \Psi_{m+1}', \ldots, \Psi_n').\end{aligned} \tag{26}$$

The last step is based on the assumption that we are able to rewrite the sum $\sum_{i,j=1}^{m}(\cdots)$ in terms of $n - m$ newly defined extensive quantities that are associated with the subsystem, to which we attribute the deviations, and are different from the $\Psi_{i,0}$, in general. In case of GWs, the wave action and the pseudomomentum may represent such quantities (see section 4c below). Equation (26) constitutes the fundamental relation of the overall system composed of the two subsystems.

Note that $\langle E \rangle$ on the lhs of Eq. (26), is not solely the energy of the subsystem *resolved atmosphere* E_0, but the energy of the overall system. By writing the fundamental relation in the form $E = \mathfrak{E}(\Psi_1, \ldots)$, we select energy as the dependent variable, while the other extensive quantities remain independent degrees of freedom. Therefore, the averaging cannot operate "freely" on the quantity *energy*, but is constrained by the fundamental relation.

In case of the GW model, which we use in this work, the fundamental relation (26) is separable insofar as $\mathfrak{E}'$ does not depend explicitly on the $\Psi_{i,0}$, i.e., $\mathfrak{E}'(\Psi_{1,0}, \ldots, \Psi_{m,0}, \Psi_{m+1}', \ldots, \Psi_n') = \mathfrak{E}'(\Psi_{m+1}', \ldots, \Psi_n')$ (for convenience, we will consider N^2 as a quasi-constant parameter of the resolved atmosphere). Therefore, we can introduce $\mathfrak{E}(\Psi_{1,0}, \ldots, \Psi_{m,0})$ and $\mathfrak{E}'$ independently in sections 4b and 4c below (cf. Falk et al. 1983).

In a next step, the differential of Eq. (26) will be combined with the budget equations of $E_0, \Psi_{1,0}, \ldots, \Psi_n'$. By defining what kind of fluxes and sources contribute to the budgets and by applying conservation and nonconservation principles, we may finally arrive at a parameterization for the effects of breaking GWs on the resolved atmosphere.

a. *Outline of the approach*

GW breaking is commonly considered an irreversible process (e.g., Medvedev and Klaassen 2003; Shaw and Shepherd 2009; Gassmann and Herzog 2015). Therefore, the methods of irreversible thermodynamics are one possible tool for its parameterization. This approach may be divided into the

following tasks (cf. Herbert 1978; Peixoto et al. 1991; Jou et al. 2001; Zdunkowski and Bott 2004; Liu et al. 2011; Gassmann and Herzog 2015; Papenfuß 2020):[4]

- Make oneself familiar with the (thermo)dynamic properties of the system at hand and express them in terms of the Gibbs equation.
- Set up budget equations for the extensive quantities contained by the system, and separate irreversible from reversible processes.
- The extensive quantity entropy is not conserved, but can be produced by irreversible processes. Combine all budget equations with the Gibbs equation to derive an expression for the source of entropy.
- From this expression, correlating thermodynamic forces and fluxes can be defined. The correlation is expressed in terms of phenomenological equations.
- If the irreversible processes are of moderate magnitude, the phenomenological equations may be linearized. The coefficients of the linear relations are the transport coefficients.
- Determine closures for the transport coefficients.

These tasks will serve as a guideline in the following.

b. Gibbs equation of the resolved atmosphere

We consider a relatively small material volume of (dry) air. Its Gibbs equation in differential form may be written (e.g., Herbert 1978; Jou et al. 2001; Zdunkowski and Bott 2004; Job and Herrmann 2006):

$$\begin{aligned}\frac{dE_0}{dt} &= \frac{\partial E_0}{\partial \mathbf{P}_0}\cdot\frac{d\mathbf{P}_0}{dt} + \frac{\partial E_0}{\partial V_0}\frac{dV_0}{dt} + \frac{\partial E_0}{\partial S_0}\frac{dS_0}{dt}\\ &= \mathbf{v}_0\cdot\frac{d\mathbf{P}_0}{dt} - p_0\frac{dV_0}{dt} + T_0\frac{dS_0}{dt}.\end{aligned} \tag{27}$$

Here, E_0, $\mathbf{P}_0$, V_0, and S_0 denote the extensive quantities energy, momentum, volume, and entropy, and $\mathbf{v}_0$, p_0, and T_0 are the intensive quantities velocity, pressure, and temperature. The mass m_0 does not occur in Eq. (27), since the mass of a material volume is conserved by definition, i.e., $dm_0/dt = 0$. Gravitational and rotational contributions to Eq. (27) are omitted for simplicity. They are less relevant to the following considerations.

Next, we assume that the material volume is sufficiently small to consider the air inside as quasi homogeneous. Employing the conservation of mass in Eq. (27) (e.g., $dE_0/dt = d(m_0e_0)/dt = m_0de_0/dt$) and dividing by the volume V_0, yields

$$\rho_0\frac{de_0}{dt} = \mathbf{v_0}\cdot\rho_0\frac{d\mathbf{p_0}}{dt} - p_0\rho_0\frac{dv_0}{dt} + T_0\rho_0\frac{ds_0}{dt}, \tag{28}$$

where $e_0 := E_0/m_0$, $\mathbf{p}_0 := \mathbf{P}_0/m_0$, $v_0 := V_0/m_0$, and $s_0 := S_0/m_0$ are mass-specific energy, momentum, volume, and entropy, and $\rho_0 := m_0/V_0$ is the density (following common practice, we will refer to mass-specific quantities Ψ/m as *specific* quantities, and to volume-specific quantities Ψ/V as *densities* in the following).

[4] In fact, we took the task list from Meixner (1960), but no English translation is available, as far as we know.

The intensive quantities depend on the extensive quantities through equations of state. Here, these are the equation of state of mechanics and two thermal equations of state (e.g., Hauf and Höller 1987; Jou et al. 2001; Zdunkowski and Bott 2004; Gassmann and Herzog 2015; Papenfuß 2020):

$$\mathbf{v}_0 = \mathbf{v}_0(\mathbf{P}_0, m_0) = \frac{\mathbf{P}_0}{m_0} = \mathbf{p}_0, \tag{29a}$$

$$\begin{aligned}T_0 &= T_0(V_0, S_0, m_0) = T_{00}\left(\frac{V_{00}}{V_0}\right)^{R/c_v} e^{(S_0 - S_{00})/(c_v m_0)}\\ &= T_{00}\left(\frac{\rho_0}{\rho_{00}}\right)^{R/c_v} e^{(s_0 - s_{00})/c_v},\end{aligned} \tag{29b}$$

$$p_0 = p_0(V_0, S_0, m_0) = \frac{m_0 R T_0}{V_0} = \rho_0 R T_0, \tag{29c}$$

where the subscript 00 denotes constant reference values, and c_v is the specific heat capacity at constant volume. Equation (29b) is equivalent to the familiar relation between specific entropy and potential temperature:

$$s_0 = s_{00} + c_p \ln\left(\frac{\theta_0}{\theta_{00}}\right). \tag{30}$$

c. Gibbs equation of the unresolved GWs

For the description of the unresolved (or subgrid-scale) GWs, we use the Wentzel–Kramers–Brillouin (WKB) approach. In this approach the GW field is spatially divided into wave packets to which dominant characteristics such as wavelength and period can be assigned. It is a widespread approach in the theoretical description of GWs and in their numerical modeling (e.g., Bretherton 1966; Jones 1969, 1971; Henyey and Pomphrey 1983; Marks and Eckermann 1995; Hasha et al. 2008; Song and Chun 2008; Muraschko et al. 2015; Amemiya and Sato 2016; Bölöni et al. 2016; Achatz et al. 2017; Song et al. 2020; Stephan et al. 2020; Bölöni et al. 2021; Kim et al. 2021; Strube et al. 2021). A scale separation between the characteristics of the resolved atmospheric state and the characteristics of the wave is one of the basic assumptions that underlies this model. That is, the variation of the resolved state has to be relatively small over a distance of the dominant wavelength [cf. Eq. (11)] and during the dominant period of the wave. This and some further requirements allow us to describe the motion of the wave packet and the evolution of the dominant wave vector with the following eikonal equations (e.g., Jones 1971; Henyey and Pomphrey 1983; Marks and Eckermann 1995; Hasha et al. 2008; Amemiya and Sato 2016; Achatz et al. 2017; Song et al. 2020):

$$\frac{d_g\mathbf{x}_{g,\pm}}{dt} = \nabla_{\mathbf{k}}\omega =: \mathbf{c}_g = \mathbf{v}_0 \pm \underbrace{\frac{1}{\hat{\omega}k_\pm^2}(\mathbf{N}^2 - \hat{\omega}^2\mathbf{l})\cdot\mathbf{k}_\pm}_{=:\hat{\mathbf{c}}_g}, \tag{31a}$$

$$\frac{d_g\mathbf{k}_\pm}{dt} = -\nabla\omega|_{\mathbf{k}_\pm\text{heldconst.}} = -(\nabla\mathbf{v}_0)\cdot\mathbf{k}_\pm \mp \nabla\hat{\omega}|_{\mathbf{k}_\pm\text{heldconst.}}. \tag{31b}$$

Here, $\mathbf{x}_{g,\pm}$ is the position of the wave packet and $\boldsymbol{\nabla}_\mathbf{k} = \partial/\partial\mathbf{k}$ stands for the derivative with respect to the wave vector. In addition, $\hat{\mathbf{c}}_g$ and $\mathbf{c}_g = \mathbf{v}_0 \pm \hat{\mathbf{c}}_g$ denote the intrinsic and extrinsic group velocities of the wave packet, respectively. The Lagrangian time derivative d_g/dt is wave packet fixed in this context, so its Eulerian expansion reads $d_g/dt = \partial/\partial + \mathbf{c}_g \cdot \boldsymbol{\nabla}$. If either the plus or minus sign is used in Eqs. (31a) depends on which sign of the root $\hat{\omega} = \sqrt{\hat{\omega}^2}$ is specified for the wave packet. In the following, we fix the positive sign, i.e., $\mathbf{x}_g = \mathbf{x}_{g,+}$ and $\mathbf{k} = \mathbf{k}_+$ (e.g., Wei et al. 2019; Bölöni et al. 2021). For the rhs expression in Eqs. (31), we used Eq. (14). The last term on the rhs of Eq. (31b), $\boldsymbol{\nabla}\hat{\omega}|_{\mathbf{k}\,\text{heldconst.}} = (\partial\hat{\omega}/\partial f^2)\boldsymbol{\nabla}f^2 + (\partial\hat{\omega}/\partial N^2)\boldsymbol{\nabla}N^2$, describes changes of the wave vector due to gradients of the Coriolis parameter and, in particular, the Brunt–Väisälä frequency (cf. Achatz et al. 2017). A nonuniform stratification may have significant effects on the propagation of GWs (e.g., Snively and Pasko 2008; Muraschko et al. 2015), but we will assume $N^2 \approx$ const. and $f^2 \approx$ const. in order to simplify the theoretical considerations in this section.

Just as there are extensive quantities contained by an air volume, mass and momentum for instance, extensive quantities may be attributed to a wave packet. Energy, wave action, and pseudomomentum are three examples. The scalar wave action can be associated with the amplitude of the wave, and it is conserved, if we consider only reversible processes and leave irreversible processes out (such as the forcing of GWs and their attenuation). So its density $\mathcal{A}$ satisfies the conservation equation (e.g., Jones 1971; Henyey and Pomphrey 1983; Marks and Eckermann 1995; Hasha et al. 2008; Amemiya and Sato 2016; Achatz et al. 2017; Song et al. 2020):

$$\frac{d_g\mathcal{A}}{dt} = -\mathcal{A}\boldsymbol{\nabla}\cdot\mathbf{c}_g. \tag{32}$$

The vectorial pseudomomentum density is related to the wave action and the wave vector via $\boldsymbol{\mathcal{P}} = \mathcal{A}\mathbf{k}$, so its budget equation follows from $\mathcal{A}$ [Eq. (31b)] + $\mathbf{k}$[Eq. (32)]:

$$\frac{d_g\boldsymbol{\mathcal{P}}}{dt} = -\boldsymbol{\mathcal{P}}\boldsymbol{\nabla}\cdot\mathbf{c}_g - (\boldsymbol{\nabla}\mathbf{v}_0)\cdot\boldsymbol{\mathcal{P}}. \tag{33}$$

Both quantities are related to the density of the energy contained by the wave packet through

$$\tilde{e}' = \mathcal{A}\hat{\omega}(\boldsymbol{\mathcal{P}}) = \mathcal{A}\left(\frac{\boldsymbol{\mathcal{P}}\cdot\mathbf{N}^2\cdot\boldsymbol{\mathcal{P}}}{\boldsymbol{\mathcal{P}}^2}\right)^{1/2}. \tag{34}$$

Here, the tilde is used to distinguish the energy density $\tilde{e} := E/V$ from the specific energy $e = E/m$ [cf. Eq. (28)]. In addition, the prime is used to distinguish this energy from the energy of the resolved atmospheric state. The intrinsic GW frequency is invariant under a scaling of the wave vector, $\hat{\omega}(\alpha\mathbf{k}) = \hat{\omega}(\mathbf{k})$ for $\alpha \neq 0$ [see Eq. (14)]. Therefore, we can write $\hat{\omega}(\mathbf{k}) = \hat{\omega}(\mathcal{A}\mathbf{k}) = \hat{\omega}(\boldsymbol{\mathcal{P}})$. The scale invariance may also be stated as $\hat{\omega}$ being homogeneous of degree zero, which implies that the intrinsic group velocity of the GW packet is perpendicular to its wave vector according to Euler's theorem (Henyey 1986):

$$\mathbf{k}\cdot\boldsymbol{\nabla}_\mathbf{k}\hat{\omega} = \mathbf{k}\cdot\hat{\mathbf{c}}_g = 0. \tag{35}$$

Note that $\mathcal{A} > 0$ holds for the positive branch of $\hat{\omega}$ and $\mathcal{A} < 0$ for the negative branch, since the energy is always positive.

To increase the accuracy with which realistic atmospheric GW fields can be described, we may need to consider a superposition of several (locally) monochromatic GWs. To cover this, we assume that n GW packets contribute to a total energy density of

$$\tilde{e}' = \sum_{j=1}^{n}\mathcal{A}_j\hat{\omega}(\boldsymbol{\mathcal{P}}_j). \tag{36}$$

Here, we make the "weak turbulence" approximation, i.e., contributions of wave–wave interactions to the total energy are neglected (e.g., Hertzog et al. 2002).

One of the disadvantages of the WKB description of GWs in physical space is the occurrence of caustics. The volume of the wave packet vanishes, where this happens, and the wave action density is no longer well-defined (Marks and Eckermann 1995; Hertzog et al. 2002; Hasha et al. 2008; Muraschko et al. 2015; Bölöni et al. 2016). For GW parameterizations that use the steady-state approximation, this is less of a problem. If, however, transient interactions between the unresolved GWs and the resolved atmosphere shall be taken into account, which cannot be covered by steady-state models, there is another solution to prevent caustics in physical space. In place of a discrete spectrum, a continuous spectrum of GWs is considered, which is formulated in the six-dimensional phase space $(\mathbf{x}, \mathbf{k})$. This means, for instance, that the expression (36) for the total energy density would be replaced by

$$\tilde{e}'(t,\mathbf{x}) = \int d^3k\mathcal{N}(t,\mathbf{x},\mathbf{k})\hat{\omega}(t,\mathbf{x},\mathbf{k}), \tag{37}$$

where $\int d^3k$ denotes the volume integral over the $\mathbf{k}$ space, and $\mathcal{N}$ is the wave action phase space density. This approach circumvents the caustics problem, since a six-dimensional volume element $d^3x d^3k$, material in terms of the wave action, is conserved (e.g., Souprayen et al. 2001; Hertzog et al. 2002; Olbers and Eden 2013; Muraschko et al. 2015; Bölöni et al. 2016). In the following, we will focus on the discrete spectrum (36), but the methods of irreversible thermodynamics could also be applied to the phase space formulation.

Finally, we consider the time derivative of Eq. (36). To make this comparable to Eq. (28), we budget the total GW energy contained by a small material air volume, and use the general relation $\rho de/dt = d\tilde{e}/dt + (\tilde{e}/v)dv/dt = d\tilde{e}/dt + \tilde{e}\boldsymbol{\nabla}\cdot\mathbf{v}$ for this purpose (e.g., Holton 2004):

$$\frac{d\tilde{e}'}{dt} + \tilde{e}'\boldsymbol{\nabla}\cdot\mathbf{v}_0 = \sum_{j=1}^{n}\left(\hat{\omega}_j\frac{d\mathcal{A}_j}{dt} + \hat{\mathbf{c}}_{gj}\cdot\frac{d\boldsymbol{\mathcal{P}}_j}{dt}\right) + \tilde{e}'\boldsymbol{\nabla}\cdot\mathbf{v}_0. \tag{38}$$

Here, we used $\hat{\omega}_j := \hat{\omega}(\mathcal{P}_j)$ and $\partial\hat{\omega}_j/\partial\mathcal{P}_j = \mathcal{A}_j^{-1}\partial\hat{\omega}_j/\partial\mathbf{k}_j = \mathcal{A}_j^{-1}\hat{\mathbf{c}}_{g,j}$. In this context, $\hat{\omega}_j$ and $\hat{\mathbf{c}}_{g,j}$ could be considered as intensive quantities, and the dispersion relation (14) as an equation of state. Now, the wave packet–fixed budget equations for wave action and pseudomomentum densities Eqs. (32) and (33) can be transformed to material-volume-fixed budgets in the following way:

$$\frac{d\mathcal{A}}{dt} = \frac{d_g\mathcal{A}}{dt} - \hat{\mathbf{c}}_g\cdot\boldsymbol{\nabla}\mathcal{A} = -\mathcal{A}\boldsymbol{\nabla}\cdot\mathbf{v}_0 - \boldsymbol{\nabla}\cdot(\hat{\mathbf{c}}_g\mathcal{A}), \tag{39a}$$

$$\frac{d\mathcal{P}}{dt} = \frac{d_g\mathcal{P}}{dt} - \hat{\mathbf{c}}_g\cdot\boldsymbol{\nabla}\mathcal{P} = -\mathcal{P}\boldsymbol{\nabla}\cdot\mathbf{v}_0 - \boldsymbol{\nabla}\cdot(\hat{\mathbf{c}}_g\mathcal{P}) - (\boldsymbol{\nabla}\mathbf{v}_0)\cdot\mathcal{P}, \tag{39b}$$

where we omitted the wave packet index j for reasons of clarity. Multiplying Eq. (39a) by $\hat{\omega}$ and Eq. (39b) by $\hat{\mathbf{c}}_g$ then yields

$$\begin{aligned}\hat{\omega}\frac{d\mathcal{A}}{dt} &= -\mathcal{A}\hat{\omega}\boldsymbol{\nabla}\cdot\mathbf{v}_0 - \hat{\omega}\boldsymbol{\nabla}\cdot(\hat{\mathbf{c}}_g\mathcal{A})\\ &= -\tilde{e}'\boldsymbol{\nabla}\cdot\mathbf{v}_0 - \boldsymbol{\nabla}\cdot(\hat{\mathbf{c}}_g\tilde{e}') + \mathcal{A}\hat{\mathbf{c}}_g\cdot\boldsymbol{\nabla}\hat{\omega},\end{aligned} \tag{40a}$$

$$\begin{aligned}\hat{\mathbf{c}}_g\cdot\frac{d\mathcal{P}}{dt} &= -(\hat{\mathbf{c}}_g\cdot\mathcal{P})\boldsymbol{\nabla}\cdot\mathbf{v}_0 - \hat{\mathbf{c}}_g\cdot[\boldsymbol{\nabla}\cdot(\hat{\mathbf{c}}_g\mathcal{P})] - \hat{\mathbf{c}}_g\cdot(\boldsymbol{\nabla}\mathbf{v}_0)\cdot\mathcal{P}\\ &= \mathcal{P}\hat{\mathbf{c}}_g\cdot\cdot\boldsymbol{\nabla}\hat{\mathbf{c}}_g - \hat{\mathbf{c}}_g\mathcal{P}\cdot\cdot(\boldsymbol{\nabla}\mathbf{v}_0)^{\mathrm{T}}.\end{aligned} \tag{40b}$$

Here, we used $\boldsymbol{\nabla}\cdot(\hat{\mathbf{c}}_g\mathcal{A}\hat{\omega}) = \hat{\omega}\boldsymbol{\nabla}\cdot(\hat{\mathbf{c}}_g\mathcal{A}) + \mathcal{A}\hat{\mathbf{c}}_g\cdot\boldsymbol{\nabla}\hat{\omega}$ for Eq. (40a), and $\hat{\mathbf{c}}_g\cdot\mathcal{P} = 0$ [see Eq. (35)] for Eq. (40b). In addition, $\hat{\mathbf{c}}_g\cdot(\boldsymbol{\nabla}\mathbf{v}_0)\cdot\mathcal{P} = \hat{\mathbf{c}}_g\mathcal{P}\cdot\cdot(\boldsymbol{\nabla}\mathbf{v}_0)^{\mathrm{T}}$ was employed [see Eq. (A1) in appendix A], and $0 = \boldsymbol{\nabla}\cdot[\hat{\mathbf{c}}_g(\mathcal{P}\cdot\hat{\mathbf{c}}_g)] = \hat{\mathbf{c}}_g\cdot[\boldsymbol{\nabla}\cdot(\hat{\mathbf{c}}_g\mathcal{P})] + \mathcal{P}\hat{\mathbf{c}}_g\cdot\cdot\boldsymbol{\nabla}\hat{\mathbf{c}}_g$ [see Eq. (B2) in appendix B]. Inserting Eqs. (40a) and (40b) in Eq. (38) finally yields

$$\frac{d\tilde{e}'}{dt} + \tilde{e}'\boldsymbol{\nabla}\cdot\mathbf{v}_0 = -\boldsymbol{\nabla}\cdot\left(\sum_{j=1}^{n}\hat{\mathbf{c}}_{g,j}\tilde{e}'_j\right) - \left(\sum_{j=1}^{n}\hat{\mathbf{c}}_{g,j}\mathcal{P}_j\right)\cdot\cdot(\boldsymbol{\nabla}\mathbf{v}_0)^{\mathrm{T}}, \tag{41}$$

where we used that the last term on the rhs of Eq. (38) and (the sum over) the first term on the rhs of Eq. (40a) cancel each other. Furthermore, $\mathcal{A}\hat{\mathbf{c}}_g\cdot\boldsymbol{\nabla}\hat{\omega} + \mathcal{P}\hat{\mathbf{c}}_g\cdot\cdot\boldsymbol{\nabla}\hat{\mathbf{c}}_g = \mathcal{A}\hat{\mathbf{c}}_g\cdot[\boldsymbol{\nabla}\hat{\omega} + (\boldsymbol{\nabla}\hat{\mathbf{c}}_g)\cdot\mathbf{k}]$ also cancels, since $\boldsymbol{\nabla}\hat{\omega} = (\boldsymbol{\nabla}\mathbf{k})\cdot\boldsymbol{\nabla}_{\mathbf{k}}\hat{\omega} = (\boldsymbol{\nabla}\mathbf{k})\cdot\hat{\mathbf{c}}_g$ (using $N^2 = \text{const.}$ and $f^2 = \text{const.}$) and the gradient of Eq. (35) yields $(\boldsymbol{\nabla}\hat{\mathbf{c}}_g)\cdot\mathbf{k} = -(\boldsymbol{\nabla}\mathbf{k})\cdot\hat{\mathbf{c}}_g$.

d. *Combined Gibbs equation, budget equations, and the source of entropy*

The Gibbs equation of the combined system, i.e., the resolved atmosphere plus the unresolved GWs, is the sum of Eqs. (28) and (38) [cf. Eq. (26)]:

$$\begin{aligned}\rho_0\frac{de_0}{dt} + \frac{d\tilde{e}'}{dt} + \tilde{e}'\boldsymbol{\nabla}\cdot\mathbf{v}_0 = \mathbf{v}_0\cdot\rho_0\frac{d\mathbf{p}_0}{dt} - p_0\rho_0\frac{dv_0}{dt} + T_0\rho_0\frac{ds_0}{dt}\\ + \sum_{j=1}^{n}\left(\hat{\omega}_j\frac{d\mathcal{A}_j}{dt} + \hat{\mathbf{c}}_{g,j}\cdot\frac{d\mathcal{P}_j}{dt}\right)\\ + \tilde{e}'\boldsymbol{\nabla}\cdot\mathbf{v}_0.\end{aligned} \tag{42}$$

Turbulence is probably an important player in the context of GW breaking, but its integration into the framework of irreversible thermodynamics is a complex problem (e.g., Blackadar 1955; Zdunkowski and Bott 2003). We will omit an explicit contribution of turbulence to the Gibbs equation, Eq. (42), since that goes beyond the scope of this work.[5]

To formulate the entropy source of the combined system, we need to define the general form of the budget equations of the extensive quantities in terms of reversible and irreversible fluxes and sources (e.g., Herbert 1978; Peixoto et al. 1991; Jou et al. 2001; Zdunkowski and Bott 2003, 2004; Holton 2004):

$$\rho_0\frac{de_0}{dt} + \frac{d\tilde{e}'}{dt} + \tilde{e}'\boldsymbol{\nabla}\cdot\mathbf{v}_0 = -\boldsymbol{\nabla}\cdot(\overset{r}{\mathbf{F}}_e + \overset{i}{\mathbf{F}}_e), \tag{43a}$$

$$\rho_0\frac{d\mathbf{p}_0}{dt} = -\boldsymbol{\nabla}\cdot(\overset{r}{\mathbf{F}}_p + \overset{i}{\mathbf{F}}_p), \tag{43b}$$

$$\rho_0\frac{dv_0}{dt} = \boldsymbol{\nabla}\cdot\mathbf{v}_0 = \mathbf{I}\cdot\cdot(\boldsymbol{\nabla}\mathbf{v}_0)^{\mathrm{T}}, \tag{43c}$$

$$\rho_0\frac{ds_0}{dt} = -\boldsymbol{\nabla}\cdot\overset{i}{\mathbf{F}}_s + \sigma_s, \tag{43d}$$

$$\frac{d\mathcal{A}_j}{dt} = [\text{rhs of Eq. (39a)}] - \boldsymbol{\nabla}\cdot\overset{i}{\mathbf{F}}_{\mathcal{A}_j} + \sigma_{\mathcal{A}_j}, \tag{43e}$$

$$\frac{d\mathcal{P}_j}{dt} = [\text{rhs of Eq. (39b)}] - \boldsymbol{\nabla}\cdot\overset{i}{\mathbf{F}}_{\mathcal{P}_j} + \boldsymbol{\sigma}_{\mathcal{P}_j} + \sigma_{\mathcal{A}_j}\mathbf{k}_j, \tag{43f}$$

where $\overset{r}{\mathbf{F}}$ and $\overset{i}{\mathbf{F}}$ denote the reversible and irreversible parts of a total flux density $\mathbf{F}$. All source densities σ are of irreversible nature. See Eq. (A1) in appendix A for the second step on the rhs of Eq. (43c). Equations (43) in words: we assume energy and momentum to be conserved locally, a material volume is reversibly changed by divergent (or convergent) winds, entropy is not conserved, but indestructible according to the second law of thermodynamics, i.e., $\sigma_s \geq 0$, finally, wave action and pseudomomentum are not conserved either, but the sign of their irreversible sources is not determined at first (for instance, $\sigma_{\mathcal{A}_j} \gtrless 0$). Reversible and irreversible processes should be independent of each other, so, when we insert the budget equations, Eqs. (43), into the Gibbs equation, Eq. (42), we can consider the reversible and irreversible parts individually. We start with the reversible part,

[5] We point, however, to the inclusive approach to turbulence modeling, where turbulent dynamics are integrated as part of the thermodynamics (e.g., Sievers 1984). If one would adopt this approach, the terms $\rho_0(T_0ds_0/dt - p_0dv_0/dt)$ on the rhs of Eq. (42) would cover both thermodynamics and the dynamics of turbulence. The ideal gas law (29c) and the caloric equation of state (29b) provide, however, only first-order (or lower) approximations with respect to turbulence (e.g., Blackadar 1955; Herbert and Kucharski 1998).

$$
\begin{aligned}
-\boldsymbol{\nabla}\cdot\overset{r}{\mathbf{F}}_e &= -\mathbf{v}_0\cdot(\boldsymbol{\nabla}\cdot\overset{r}{\mathbf{F}}_p) - p_0\mathbf{I}\cdot\cdot(\boldsymbol{\nabla}\mathbf{v}_0)^{\mathrm{T}} \\
&\quad - \boldsymbol{\nabla}\cdot\left(\sum_{j=1}^{n}\hat{\mathbf{c}}_{g,j}\tilde{e}'_j\right) - \left(\sum_{j=1}^{n}\hat{\mathbf{c}}_{g,j}\boldsymbol{\mathcal{P}}_j\right)\cdot\cdot(\boldsymbol{\nabla}\mathbf{v}_0)^{\mathrm{T}} \\
&= -\boldsymbol{\nabla}\cdot\left(\overset{r}{\mathbf{F}}_p\cdot\mathbf{v}_0 + \sum_{j=1}^{n}\hat{\mathbf{c}}_{g,j}\tilde{e}'_j\right) \\
&\quad + \underbrace{\left(\overset{r}{\mathbf{F}}_p - p_0\mathbf{I} - \sum_{j=1}^{n}\hat{\mathbf{c}}_{g,j}\boldsymbol{\mathcal{P}}_j\right)\cdot\cdot(\boldsymbol{\nabla}\mathbf{v}_0)^{\mathrm{T}}}_{=0}, \qquad (44)
\end{aligned}
$$

where we used Eq. (41) in the first step, and $\mathbf{v}_0\cdot(\boldsymbol{\nabla}\cdot\overset{r}{\mathbf{F}}_p) = \boldsymbol{\nabla}\cdot(\overset{r}{\mathbf{F}}_p\cdot\mathbf{v}_0) - \overset{r}{\mathbf{F}}_p\cdot\cdot(\boldsymbol{\nabla}\mathbf{v}_0)^{\mathrm{T}}$[see Eq. (B1) in appendix B] in the second step. Energy conservation requires that the second term on the rhs vanishes for arbitrary $(\boldsymbol{\nabla}\mathbf{v}_0)^{\mathrm{T}}$. Therefore, the reversible momentum flux density reads[6]

$$
\overset{r}{\mathbf{F}}_p = p_0\mathbf{I} + \sum_{j=1}^{n}\hat{\mathbf{c}}_{g,j}\boldsymbol{\mathcal{P}}_j. \qquad (45)
$$

Next, we consider the irreversible part:

$$
\begin{aligned}
-\boldsymbol{\nabla}\cdot\overset{i}{\mathbf{F}}_e &= -\mathbf{v}_0\cdot(\boldsymbol{\nabla}\cdot\overset{i}{\mathbf{F}}_p) - T_0\boldsymbol{\nabla}\cdot\overset{i}{\mathbf{F}}_s + T_0\sigma_s \\
&\quad + \sum_{j=1}^{n}[-\hat{\omega}_j\boldsymbol{\nabla}\cdot\overset{i}{\mathbf{F}}_{\mathcal{A}_j} + \sigma_{\mathcal{A}_j}\hat{\omega}_j - \hat{\mathbf{c}}_{g,j}\cdot(\boldsymbol{\nabla}\cdot\overset{i}{\mathbf{F}}_{\boldsymbol{\mathcal{P}}_j}) + \boldsymbol{\sigma}_{\boldsymbol{\mathcal{P}}_j}\cdot\hat{\mathbf{c}}_{g,j}] \\
&= -\boldsymbol{\nabla}\cdot[\overset{i}{\mathbf{F}}_p\cdot\mathbf{v}_0 + T_0\overset{i}{\mathbf{F}}_s + \sum_{j=1}^{n}(\hat{\omega}_j\overset{i}{\mathbf{F}}_{\mathcal{A}_j} + \overset{i}{\mathbf{F}}_{\boldsymbol{\mathcal{P}}_j}\cdot\hat{\mathbf{c}}_{g,j})] \\
&\quad + \overset{i}{\mathbf{F}}_p\cdot\cdot(\boldsymbol{\nabla}\mathbf{v}_0)^{\mathrm{T}} + \overset{i}{\mathbf{F}}_s\cdot\boldsymbol{\nabla}T_0 + T_0\sigma_s \\
&\quad + \sum_{j=1}^{n}[\overset{i}{\mathbf{F}}_{\mathcal{A}_j}\cdot\boldsymbol{\nabla}\hat{\omega}_j + \sigma_{\mathcal{A}_j}\hat{\omega}_j + \overset{i}{\mathbf{F}}_{\boldsymbol{\mathcal{P}}_j}\cdot\cdot(\boldsymbol{\nabla}\hat{\mathbf{c}}_{g,j})^{\mathrm{T}} + \boldsymbol{\sigma}_{\boldsymbol{\mathcal{P}}_j}\cdot\hat{\mathbf{c}}_{g,j}]. \qquad (46)
\end{aligned}
$$

The term $\sigma_{\mathcal{A}_j}\mathbf{k}_j$ on the rhs of Eq. (43f) does not contribute to Eq. (46), since wave vector and intrinsic group velocity are perpendicular to each other [see Eq. (35)]. Again, the conservation of energy requires that those rhs terms, which are not expressed as the divergence of a flux, vanish. This may be achieved by choosing the following expression for the entropy source density (times the temperature):

$$
\begin{aligned}
T_0\sigma_s &= -\overset{i}{\mathbf{F}}_p\cdot\cdot(\boldsymbol{\nabla}\mathbf{v}_0)^{\mathrm{T}} - \overset{i}{\mathbf{F}}_s\cdot\boldsymbol{\nabla}T_0 \\
&\quad - \sum_{j=1}^{n}[\overset{i}{\mathbf{F}}_{\mathcal{A}_j}\cdot\boldsymbol{\nabla}\hat{\omega}_j + \sigma_{\mathcal{A}_j}\hat{\omega}_j + \overset{i}{\mathbf{F}}_{\boldsymbol{\mathcal{P}}_j}\cdot\cdot(\boldsymbol{\nabla}\hat{\mathbf{c}}_{g,j})^{\mathrm{T}} \\
&\quad + \boldsymbol{\sigma}_{\boldsymbol{\mathcal{P}}_j}\cdot\hat{\mathbf{c}}_{g,j}] \geq 0. \qquad (47)
\end{aligned}
$$

The dissipation (47) has to be nonnegative according to the second law of thermodynamics. It provides the basis for the parameterization of irreversible processes (e.g., Herbert 1978; Peixoto et al. 1991; Jou et al. 2001; Zdunkowski and Bott 2004; Gassmann and Herzog 2015; Papenfuß 2020).

e. Phenomenological equations

The factors $(\boldsymbol{\nabla}\mathbf{v}_0)^{\mathrm{T}}$, $\boldsymbol{\nabla}T_0$, $\boldsymbol{\nabla}\hat{\omega}_j$, $\hat{\omega}_j$, $(\boldsymbol{\nabla}\hat{\mathbf{c}}_{g,j})^{\mathrm{T}}$, and $\hat{\mathbf{c}}_{g,j}$ on the rhs of Eq. (47) are available quantities and they are called *thermodynamic forces*. The irreversible flux and source densities, $\overset{i}{\mathbf{F}}_p$, $\overset{i}{\mathbf{F}}_s$, $\overset{i}{\mathbf{F}}_{\mathcal{A}_j}$, $\overset{i}{\mathbf{F}}_{\boldsymbol{\mathcal{P}}_j}$, $\sigma_{\mathcal{A}_j}$, and $\boldsymbol{\sigma}_{\boldsymbol{\mathcal{P}}_j}$, on the other hand, are placeholders for which expressions have yet to be found. It is assumed that these fluxes and sources are functions of the thermodynamic forces, e.g., $\overset{i}{\mathbf{F}}_p = \overset{i}{\mathbf{F}}_p[(\boldsymbol{\nabla}\mathbf{v}_0)^{\mathrm{T}}, \boldsymbol{\nabla}T_0, \boldsymbol{\nabla}\hat{\omega}_j, \hat{\omega}_j, (\boldsymbol{\nabla}\hat{\mathbf{c}}_{g,j})^{\mathrm{T}}, \hat{\mathbf{c}}_{g,j}]$. If the system would approach thermodynamic equilibrium, i.e., $T_0\sigma_s \to 0$, the thermodynamic forces and the fluxes and sources have to vanish simultaneously. Provided the irreversible processes can be considered relatively small deviations from the equilibrium, the dependence on the forces may be linearized. The approximate flux densities then read (Onsager 1931; Herbert 1978; Jou et al. 2001; Zdunkowski and Bott 2004; Gassmann and Herzog 2015; Papenfuß 2020)[7]

$$
\begin{aligned}
\overset{i}{\mathbf{F}}_p &= \underline{-\mathbf{L}^{(4)}_{\alpha}\cdot\cdot(\boldsymbol{\nabla}\mathbf{v}_0)^{\mathrm{T}}} - \mathbf{L}^{(3)}_{\alpha\beta}\cdot\boldsymbol{\nabla}T_0 \\
&\quad - \sum_{j=1}^{n}[\mathbf{L}^{(3)}_{\alpha\gamma,j}\cdot\boldsymbol{\nabla}\hat{\omega}_j + \mathbf{L}_{\alpha\epsilon,j}\hat{\omega}_j + \mathbf{L}^{(4)}_{\alpha\delta,j}\cdot\cdot(\boldsymbol{\nabla}\hat{\mathbf{c}}_{g,j})^{\mathrm{T}} \\
&\quad + \mathbf{L}^{(3)}_{\alpha\zeta,j}\cdot\hat{\mathbf{c}}_{g,j}], \qquad (48a) \\
\overset{i}{\mathbf{F}}_s &= \underline{-\mathbf{L}_{\beta}\cdot\boldsymbol{\nabla}T_0} - \mathbf{L}^{(3)}_{\beta\alpha}\cdot\cdot(\boldsymbol{\nabla}\mathbf{v}_0)^{\mathrm{T}} \\
&\quad - \sum_{j=1}^{n}[\mathbf{L}_{\beta\gamma,j}\cdot\boldsymbol{\nabla}\hat{\omega}_j + \mathbf{L}_{\beta\epsilon,j}\hat{\omega}_j + \mathbf{L}^{(3)}_{\beta\delta,j}\cdot\cdot(\boldsymbol{\nabla}\hat{\mathbf{c}}_{g,j})^{\mathrm{T}} \\
&\quad + \mathbf{L}_{\beta\zeta,j}\cdot\hat{\mathbf{c}}_{g,j}], \qquad (48b) \\
\overset{i}{\mathbf{F}}_{\mathcal{A}_j} &= \underline{-\mathbf{L}_{\gamma,j}\cdot\boldsymbol{\nabla}\hat{\omega}_j} - \mathbf{L}^{(3)}_{\gamma\alpha,j}\cdot\cdot(\boldsymbol{\nabla}\mathbf{v}_0)^{\mathrm{T}} - \mathbf{L}_{\gamma\beta,j}\cdot\boldsymbol{\nabla}T_0 \\
&\quad - \sum_{k=1}^{n}[\mathbf{L}_{\gamma\gamma,j,k}\cdot\boldsymbol{\nabla}\hat{\omega}_k|_{k\neq j} + \mathbf{L}_{\gamma\epsilon,j,k}\hat{\omega}_k \\
&\quad + \mathbf{L}^{(3)}_{\gamma\delta,j,k}\cdot\cdot(\boldsymbol{\nabla}\hat{\mathbf{c}}_{g,k})^{\mathrm{T}} + \mathbf{L}_{\gamma\zeta,j,k}\cdot\hat{\mathbf{c}}_{g,k}], \qquad (48c) \\
\overset{i}{\mathbf{F}}_{\boldsymbol{\mathcal{P}}_j} &= \underline{-\mathbf{L}^{(4)}_{\delta,j}\cdot\cdot(\boldsymbol{\nabla}\hat{\mathbf{c}}_{g,j})^{\mathrm{T}}} - \mathbf{L}^{(4)}_{\delta\alpha,j}\cdot\cdot(\boldsymbol{\nabla}\mathbf{v}_0)^{\mathrm{T}} - \mathbf{L}^{(3)}_{\delta\beta,j}\cdot\boldsymbol{\nabla}T_0 \\
&\quad - \sum_{k=1}^{n}[\mathbf{L}^{(3)}_{\delta\gamma,j,k}\cdot\boldsymbol{\nabla}\hat{\omega}_k + \mathbf{L}_{\delta\epsilon,j,k}\hat{\omega}_k \\
&\quad + \mathbf{L}^{(4)}_{\delta\delta,j,k}\cdot\cdot(\boldsymbol{\nabla}\hat{\mathbf{c}}_{g,k})^{\mathrm{T}}|_{k\neq j} + \mathbf{L}^{(3)}_{\delta\zeta,j,k}\cdot\hat{\mathbf{c}}_{g,k}], \qquad (48d)
\end{aligned}
$$

[6] The momentum flux tensor is not symmetric, since $\sum_j\hat{\mathbf{c}}_{g,j}\boldsymbol{\mathcal{P}}_j \neq \sum_j(\hat{\mathbf{c}}_{g,j}\boldsymbol{\mathcal{P}}_j)^{\mathrm{T}} = \sum_j\boldsymbol{\mathcal{P}}_j\hat{\mathbf{c}}_{g,j}$, in general. This violates the conservation of orbital angular momentum {with density $\rho[\mathbf{r}\times(\boldsymbol{\Omega}\times\mathbf{r}+\mathbf{v}_0)]$, where $\mathbf{r}$ denotes the distance relative to the center of Earth}. A skew-symmetric part of the momentum flux tensor provides a source/sink of orbital angular momentum and, at the same time, a sink/source of spin angular momentum, so that the total angular momentum (=orbital angular momentum + spin angular momentum) is still conserved. It is, however, common practice in atmospheric physics to ignore the budget of spin angular momentum of an air volume. Therefore, the total angular momentum is effectively equal to the orbital angular momentum, and any source/sink of the latter violates the conservation of the former (e.g., Herbert 1978; Zdunkowski and Bott 2003).

[7] A simple example may illustrate this more clearly. Consider a system with two irreversible scalar flux densities F_α and F_β, and the corresponding thermodynamic forces X_α and X_β, so that $T\sigma_s = -F_\alpha X_\alpha - F_\beta X_\beta$. Linearizing the phenomenological equations $F_{\alpha/\beta} = F_{\alpha/\beta}(X_\alpha, X_\beta)$ about thermodynamic equilibrium $X_{\alpha/\beta} = 0$ yields $F_\alpha \approx (\partial F_\alpha/\partial X_\alpha)X_\alpha + (\partial F_\alpha/\partial X_\beta)X_\beta = -L_{\alpha\alpha}X_\alpha - L_{\alpha\beta}X_\beta$ and $F_\beta \approx (\partial F_\beta/\partial X_\alpha)X_\alpha + (\partial F_\beta/\partial X_\beta)X_\beta = -L_{\beta\alpha}X_\alpha - L_{\beta\beta}X_\beta$. The L coefficients are called transport coefficients. In addition, $(-L_{\alpha\alpha}X_\alpha)$ and $(-L_{\beta\beta}X_\beta)$ are called the direct effects (for their coefficients, we would use the abbreviations $L_{\alpha\alpha} \to L_\alpha$ and $L_{\beta\beta} \to L_\beta$), and $(-L_{\alpha\beta}X_\beta)$ and $(-L_{\beta\alpha}X_\alpha)$ are the cross effects (see, e.g., Onsager 1931).

and for the source densities we obtain

$$\sigma_{\mathcal{A}_j} = \underline{-L_{\epsilon,j}\hat{\omega}_j} - \mathbf{L}_{\epsilon\alpha,j}\cdot\cdot(\boldsymbol{\nabla}\mathbf{v}_0)^{\mathrm{T}} - \mathbf{L}_{\epsilon\beta,j}\cdot\boldsymbol{\nabla}T_0 - \sum_{k=1}^{n}[\mathbf{L}_{\epsilon\gamma,j,k}\cdot\boldsymbol{\nabla}\hat{\boldsymbol{\omega}}_k + L_{\epsilon\epsilon,j,k}\hat{\boldsymbol{\omega}}_k|_{k\neq j} + \mathbf{L}_{\epsilon\delta,j,k}\cdot\cdot(\boldsymbol{\nabla}\hat{\mathbf{c}}_{g,k})^{\mathrm{T}} + \mathbf{L}_{\epsilon\zeta,j,k}\cdot\hat{\mathbf{c}}_{g,k}], \tag{49a}$$

$$\boldsymbol{\sigma}_{\mathcal{P}_j} = \underline{-\mathbf{L}_{\zeta,j}\cdot\hat{\mathbf{c}}_{g,j}} - \mathbf{L}^{(3)}_{\zeta\alpha,j}\cdot\cdot(\boldsymbol{\nabla}\mathbf{v}_0)^{\mathrm{T}} - \mathbf{L}_{\zeta\beta,\mathrm{j}}\cdot\boldsymbol{\nabla}T_0 - \sum_{k=1}^{n}[\mathbf{L}_{\zeta\gamma,j,k}\cdot\boldsymbol{\nabla}\hat{\boldsymbol{\omega}}_k + \mathbf{L}_{\zeta\epsilon,j,k}\hat{\boldsymbol{\omega}}_k + \mathbf{L}^{(3)}_{\zeta\delta,j,k}\cdot\cdot(\boldsymbol{\nabla}\hat{\mathbf{c}}_{g,k})^{\mathrm{T}} + \mathbf{L}_{\zeta\zeta,j,k}\cdot\hat{\mathbf{c}}_{g,k}|_{k\neq j}]. \tag{49b}$$

Here, L and $\mathbf{L} = \sum_{i=1}^{3} L_i\mathbf{e}_i$ denote scalar and vectorial transport coefficients, where the $\mathbf{e}_i$ are the unit vectors of an arbitrary normal basis. In addition, $\mathbf{L} = \sum_{i,j=1}^{3} L_{ij}\mathbf{e}_i\mathbf{e}_j$, $\mathbf{L}^{(3)} = \sum_{i,j,k=1}^{3} L_{ijk}\mathbf{e}_i\mathbf{e}_j\mathbf{e}_k$, and $\mathbf{L}^{(4)} = \sum_{i,j,k,l=1}^{3} L_{ijkl}\mathbf{e}_i\mathbf{e}_j\mathbf{e}_k\mathbf{e}_l$ are tensorial transport coefficients of second, third, and fourth order. Products of coefficients and forces may be evaluated as follows: $\mathbf{L}^{(3)}\cdot\mathbf{a} = L_{ijk}a_l\mathbf{e}_i\mathbf{e}_j\mathbf{e}_k\cdot\mathbf{e}_l = L_{ijk}a_k\mathbf{e}_i\mathbf{e}_j$ and $\mathbf{L}^{(3)}\cdot\cdot\mathbf{A} = L_{ijk}A_{lm}\mathbf{e}_i\mathbf{e}_j\mathbf{e}_k\cdot\cdot\mathbf{e}_l\mathbf{e}_m = L_{ijk}A_{lm}\mathbf{e}_i(\mathbf{e}_k\cdot\mathbf{e}_l)(\mathbf{e}_j\cdot\mathbf{e}_m) = L_{ijk}A_{kj}\mathbf{e}_i$ for arbitrary vector $\mathbf{a}$ and second-order tensor $\mathbf{A}$ [for brevity, we omitted the sigma sign, see Eq. (A1) in appendix A]. Products with coefficients $\mathbf{L}$ and $\mathbf{L}^{(4)}$ can be evaluated analogously. Finally, $|_{k\neq j}$ indicates that the preceding term is dropped for $k = j$. The transport coefficients may depend on ρ_0, s_0, $\mathbf{p}_0$, e_0, $\mathcal{A}_j$, $\mathcal{P}_j$, $\tilde{e}'$, the gravity $\boldsymbol{\nabla}\Phi$, the angular velocity of Earth $\boldsymbol{\Omega}$, and other parameters, but they do not depend on the thermodynamic forces. The underlined rhs terms are the direct forcing of the fluxes and sources through their corresponding conjugate forces [e.g., $(\boldsymbol{\nabla}\mathbf{v}_0)^{\mathrm{T}}$ is the corresponding conjugate force of the momentum flux $\overset{i}{\mathbf{F}}_p$, and $\boldsymbol{\nabla}T_0$ corresponds to $\overset{i}{\mathbf{F}}_s$]. The terms that are not underlined describe cross effects. These terms occur in pairs, for example, the second rhs terms of Eqs. (48a) and (48b), with transport coefficients $\mathbf{L}^{(3)}_{\alpha\beta}$ and $\mathbf{L}^{(3)}_{\beta\alpha}$ form a pair. In general, a cross effect with coefficient L_{yx} is the partner of the cross effect with coefficient L_{xy}. These cross effect terms make it possible to model, for instance, the case that a wind gradient $(\boldsymbol{\nabla}\mathbf{v}_0)^{\mathrm{T}}$ forces not only a momentum flux, but also a heat flux, and vice versa, a temperature gradient $\boldsymbol{\nabla}T_0$ forces both heat and momentum fluxes. When we consider GWs, cross effects proportional to wind and temperature gradients in Eqs. (48c)–(49b) could perhaps be used to parameterize such processes as the forcing of GWs by jet–front systems (e.g., Amiramjadi et al. 2020). In general, both partners of a cross effect pair should be taken into account, since it may need the contributions of both to the dissipation (47) to ensure it being nonnegative in all circumstances.

Working with Eqs. (48) and (49) without additional constraints for the transport coefficients would be hopelessly complicated. A fourth-order tensor alone has $3^4 = 81$ independent components. There are, however, some "natural" constraints. First, the coefficients have to be chosen in accordance with the second law of thermodynamics (47). Second, the transport coefficients of the momentum flux $\overset{i}{\mathbf{F}}_p$ have to respect its symmetry (the pseudomomentum flux $\overset{i}{\mathbf{F}}_{\mathcal{P}_j}$, in contrast, is not necessarily symmetric). Third, we may apply the *Onsager–Casimir reciprocal relations* that relate the two transport coefficients of a cross effect pair to each other (e.g., $\mathbf{L}^{(3)}_{\alpha\beta}$ is related to $\mathbf{L}^{(3)}_{\beta\alpha}$). Apart from this, the problem significantly simplifies if the medium is approximately isotropic. If this is the case, fluxes and sources can only be forced by thermodynamic forces of the same tensor order (*principle of Curie*; see, e.g., Herbert 1978; Jou et al. 2001; Zdunkowski and Bott 2004). As a result, most cross effects vanish. For the momentum flux, for instance, isotropic conditions yield

$$\begin{aligned}\overset{i}{\mathbf{F}}_p &= -\mathbf{L}^{(4)}_{\alpha}\cdot\cdot(\boldsymbol{\nabla}\mathbf{v}_0)^{\mathrm{T}} - \sum_{j=1}^{n}\mathbf{L}^{(4)}_{\alpha\delta j}\cdot\cdot(\boldsymbol{\nabla}\hat{\mathbf{c}}_{g,j})^{\mathrm{T}}\\ &= -L_1\,\mathrm{dev}(\boldsymbol{\nabla}\mathbf{v}_0^{\mathrm{T}}) - L_2\,\mathrm{sph}(\boldsymbol{\nabla}\mathbf{v}_0^{\mathrm{T}}) - L_3\,\mathrm{skw}(\boldsymbol{\nabla}\mathbf{v}_0^{\mathrm{T}})\\ &\quad - \sum_{j=1}^{n}[L_{4,j}\,\mathrm{dev}(\boldsymbol{\nabla}\hat{\mathbf{c}}_{g,j}^{\mathrm{T}}) + L_{5,j}\,\mathrm{sph}(\boldsymbol{\nabla}\hat{\mathbf{c}}_{g,j}^{\mathrm{T}}) + L_{6,j}\,\mathrm{skw}(\boldsymbol{\nabla}\hat{\mathbf{c}}_{g,j}^{\mathrm{T}})],\end{aligned} \tag{50}$$

where dev(), sph(), and skw() denote the deviatoric, the spherical (or isotropic), and the skew-symmetric parts of a second-order tensor, respectively [see Eqs. (C1) and (C2) in appendix C]. The first two transport coefficients bear established names, $L_1/2$ is the shear viscosity, and $L_2/3$ is the bulk (or volume) viscosity. (Note that we do not explicitly discriminate between molecular and turbulent (or eddy) transport coefficients, here.) In general, skew-symmetric parts will be excluded from the rhs of Eq. (50), because they lead to a violation of the conservation of orbital angular momentum (e.g., Herbert 1978; Zdunkowski and Bott 2003). This means that the coefficients L_3 and $L_{6,j}$ will be set equal to zero. As for the atmosphere, we may assume isotropic conditions on the microscale. In general, however, the atmosphere shows a number of preferred directions that could lead to anisotropic relations between the forces and the fluxes and sources. Gravity $\boldsymbol{\nabla}\Phi$, Earth's angular velocity $\boldsymbol{\Omega}$, wind $\mathbf{v}_0$, and wave vectors $\mathbf{k}_j$, for instance, can constitute such preferred directions.[8] The GW-driven irreversible processes, in particular, may be expected to be anisotropic, since their dispersion relation (14) already contains an anisotropy between the vertical and the horizontal.

In the following, we have to limit the consideration to a subset of the irreversible processes. We cannot rule out that important subprocesses associated with GW breaking may be

[8] Consider a coarsely resolved general circulation model, used for climate projections, for instance, where $\overset{i}{\mathbf{F}}_s$ could represent the eddy heat flux density. A temperature gradient, of equal strength in vertical and horizontal directions, could then force vertical and horizontal eddy fluxes of different strength, (large-scale) winds could affect these fluxes, and the Coriolis acceleration could deflect them. This might be expressed by $\overset{i}{\mathbf{F}}_s = -\mathbf{L}_\beta\cdot\boldsymbol{\nabla}T_0 = -[L_z\mathbf{e}_z\mathbf{e}_z + L_h(\mathbf{I} - \mathbf{e}_z\mathbf{e}_z) + L_\parallel\mathbf{v}_0\mathbf{v}_0 + L_\perp(\mathbf{v}_0^2\mathbf{I} - \mathbf{v}_0\mathbf{v}_0) + L_{\circlearrowleft}\mathbf{W}]\cdot\boldsymbol{\nabla}T_0$, where $\mathbf{I} - \mathbf{e}_z\mathbf{e}_z = \mathbf{e}_x\mathbf{e}_x + \mathbf{e}_y\mathbf{e}_y$ is the horizontal identity tensor, and $\mathbf{W} = \boldsymbol{\Omega}\times\mathbf{I}$ is the angular velocity tensor. The coefficients L_h and L_z would stand for the common horizontal and vertical thermal eddy conductivities, $L_\parallel$ and $L_\perp$ would be the coefficients of down- and crosswind modifications, and $L_{\circlearrowleft}$ would control the strength of the Coriolis deflection (compare Herbert 1978; Jou et al. 2001).

parameterized by the fluxes (48c) and (48d), but their treatment is simply too extensive and complex to fit in the scope of this work. Perhaps most essential for the parameterization of the wave breaking seem to us the irreversible wave action and pseudomomentum sources, (49a) and (49b); therefore, we will focus on them in the remainder of this work. In addition, we assume that the cross effects, of which the irreversible wave–wave interactions are perhaps particularly relevant, are less important than the direct effects. This means that we will base the further steps of the parameterization on the following expressions:

$$\sigma_{\mathcal{A}_j} = -L_{\epsilon,j}\hat{\omega}_j, \quad \boldsymbol{\sigma}_{\boldsymbol{\mathcal{P}}_j} = -\mathbf{L}_{\zeta,j}\cdot\hat{\mathbf{c}}_{g,j}, \tag{51a}$$

$$T_0\sigma_s = \sum_{j=1}^{n}(L_{\epsilon,j}\hat{\omega}_j^2 + \hat{\mathbf{c}}_{g,j}\cdot\mathbf{L}_{\zeta,j}\cdot\hat{\mathbf{c}}_{g,j}) \geq 0. \tag{51b}$$

There are parameterizations of GW breaking that take an effect on the transport coefficients $\mathbf{L}_\alpha^{(4)}$ and $\mathbf{L}_\beta$ [see Eqs. (48a) and (48b)] into account (e.g., Lindzen 1981; Hines 1997). This aspect is, however, not considered in this work.

f. Closures for the transport coefficients

According to Eq. (51b), the second law requires the transport coefficients $L_{\epsilon,j}$ and $\mathbf{L}_{\zeta,j}$ to be positive definite, but apart from that, no further restrictions on their form are made. At this point, input from other approaches is required (Herbert 1978; Jou et al. 2001). There are countless lines of reasoning one could follow to arrive at a model approach for the transport coefficients. For instance, any methodology applied to determine turbulent transport coefficients could be transferred to the problem at hand, in principle. Here, we follow a relatively simple heuristic approach, but we emphasize that it is only one possibility out of a probably infinite set of possible approaches. To narrow down the form of the closure, we see basically four elements. First, we want to avoid a closer investigation of the spatial structure of the instability in this work. Therefore, we assume isotropic transport coefficients in that $\mathbf{L}_{\zeta,j} = L_{\zeta,j}\mathbf{I}$. As a result, $\boldsymbol{\sigma}_{\boldsymbol{\mathcal{P}}_j}$ is perpendicular to $\boldsymbol{\mathcal{P}}_j$ [see Eq. (35)], so that its effect is limited to changes of direction. Second, as it is common practice to set turbulent transport coefficients proportional to the density (e.g., Gassmann and Herzog 2015), we will set the coefficients proportional to the wave action density, i.e., $L_{\epsilon,j}, L_{\zeta,j} \propto \mathcal{A}_j$. In this way, the forcing vanishes as the "amount" of GW vanishes. Third, we assume the greater the instability the stronger is the damping of the GWs. Therefore, the transport coefficients should be proportional to a quantity that measures the strength of the instability. Its inverse time scale $\mathcal{T}_{\text{in}}^{-1}$ [see Eq. (24)] is a possible candidate for this purpose. The greater the instability the shorter is its time scale and the larger its inverse. Finally, we incorporate the *wave period criterion* of Hines (1971, 1988), according to which the instability could only result in significant wave breaking, if the wave period is comparable to or longer than the instability time scale (see also Marks and Eckermann 1995).

To determine this time scale, we need the GW amplitude in terms of the Exner pressure [see Eq. (22b)]. Using the following relation (e.g., Muraschko et al. 2015; Bölöni et al. 2016; Achatz et al. 2017),

$$\tilde{e}' = \mathcal{A}\hat{\omega} = \frac{\rho_0 g^2}{2N^2\theta_0^2}|\hat{\theta}|^2 = \frac{\rho_0 c_p^2\theta_0^2 k_z^2}{2N^2}\frac{k^4}{k_z^4}|\hat{\pi}|^2, \tag{52}$$

we may express the modulus of the Exner pressure amplitude in terms of the wave action density [see Eq. (15) for the last step in Eq. (52)]. Now, there are at least two possible ways of preceding in case of the discrete GW spectrum (36). First, we could assume that each GW breaks as if other GW packets were not present. In this case, we can use Eqs. (22b) and (52) for computing individual instability time scales. By contrast, there could be a collective process of breaking, controlled by a single time scale that results from the superposition of all GW packets (cf. Bölöni et al. 2021):

$$\mathbf{S}' = -\sum_{j=1}^{n}\mathbf{k}_j\mathbf{k}_j\frac{k_{z,j}^2}{k_j^2}\sqrt{\frac{2N^2\hat{\omega}_j\mathcal{A}_j}{\rho_0 k_{z,j}^2}}, \tag{53}$$

where we used Eq. (20). This expression is likely a rather conservative estimate of $\mathbf{S}'$ for the most unstable configuration that could arise from the superposition of the GWs. Estimates that are more sophisticated are difficult, since the phase relations of the GWs among themselves are unknown in the WKB approach. Equation (53) is, however, in line with the weak turbulence approximation. This second option is more complex, since, in contrast to a monochromatic GW, the coefficient c of the characteristic Eq. (9) does not vanish in general, so that the equation preserves its cubic character [cf. Eqs. (21)]. This makes it more difficult to solve for its roots. From a purely computational point of view, however, solving for the n individual time scales would probably become more expensive than solving for the single collective time scale above a certain value for n. The last element of the closure is the wave period criterion. It says that instabilities could only result in significant wave breaking, if the wave period is comparable to or longer than a multiple of the instability time scale, i.e., $\mathcal{T}_{\text{GW}}/(m\mathcal{T}_{\text{in}}) > 1$ is required, where $m\mathcal{T}_{\text{in}}$ denotes the multiple of the instability time scale (with $m > 0$). To account for this, we will multiply by the following shape factor:

$$\Lambda(\tau, m) = \frac{\tau/m}{1 + \tau/m} = \frac{\tau}{m + \tau}; \tag{54}$$

see Eq. (24) for the definition of τ. It satisfies $\Lambda \to 0$ for $\tau \to 0$ and $\Lambda \to 1$ for $\tau \to \infty$ (the latter the faster the smaller the value of m). With this, we may formulate the following relaxation ansatzes for Eq. (51a):

$$\sigma_{\mathcal{A}_j} = -L_{\epsilon,j}\hat{\omega}_j = -\frac{K_\epsilon}{2\pi}\Lambda(\tau_j, m)\tau_j\mathcal{A}_j\hat{\omega}_j = -K_\epsilon\Lambda_j\frac{\mathcal{A}_j}{\mathcal{T}_{\text{in},j}}, \tag{55a}$$

$$\begin{aligned}\boldsymbol{\sigma}_{\boldsymbol{\mathcal{P}}_j} &= -L_{\zeta,j}\hat{\mathbf{c}}_{g,j} = -\frac{K_\zeta}{2\pi}\Lambda_j\tau_j\mathcal{A}_j\frac{\hat{\omega}_j^4 k_j^2}{(N^2 - \hat{\omega}_j^2)(\hat{\omega}_j^2 - f^2)}\hat{\mathbf{c}}_{g,j}\\ &= -K_\zeta\Lambda_j\mathbf{M}\cdot\mathcal{T}_{\text{in},j}^{-1}\boldsymbol{\mathcal{P}}_j,\end{aligned} \tag{55b}$$

$$T_0\sigma_s = (K_\epsilon + K_\zeta)\sum_{j=1}^{n}\frac{\Lambda_j\mathcal{A}_j\hat{\omega}_j}{\mathcal{T}_{\text{in},j}}, \tag{55c}$$

where the second-order tensor $\mathbf{M}$ can be expanded according to $\mathbf{M} = \hat{\omega}_j^2(\hat{\omega}_j^2 - f^2)^{-1}(\mathbf{e}_x + \mathbf{e}_y) - \hat{\omega}_j^2(N^2 - \hat{\omega}_j^2)^{-1}\mathbf{e}_z$ in Cartesian coordinates. If we write $L_{\zeta,j} = (K_\zeta/K_\epsilon)L_{\epsilon,j}\chi_j$ for the pseudomomentum transport coefficient, it was not obvious to us how an expression for the factor χ_j could look like (the dimension of $L_{\zeta,j}$ requires such factor). We arbitrarily selected that $\boldsymbol{\sigma}_{\mathcal{P}_j}$ should contribute to the dissipation (51b) as much as $\sigma_{\mathcal{A}_j}$ does (if we set $K_\zeta = K_\epsilon$). In combination with the definition of $\hat{\mathbf{c}}_g$ in Eq. (31a) and $\hat{c}_g^2 = \hat{\mathbf{c}}_g \cdot \hat{\mathbf{c}}_g = (N^2 - \hat{\omega}^2)(\hat{\omega}^2 - f^2)/(\hat{\omega}^2 k^2)$, Eq. (55b) follows. The coefficients K_ϵ and K_ζ are tunable nondimensional parameters, which we assume to be independent of the properties of single GW packets. If the relaxation ansatz (55) provides an adequate description of the dissipation through GW breaking, K_ϵ and K_ζ should be of order 1.[9] Equations (55) differ in at least two points from the common phenomenological approach. First, we saw in section 4e that the transport coefficients do not depend on the thermodynamic forces, since the phenomenological equations are linearized about thermodynamic equilibrium. Here, we could not satisfy this requirement, $L_{\epsilon,j}$ and $L_{\zeta,j}$ do depend on $\hat{\omega}_j$ and $\hat{\mathbf{c}}_{g,j}$(as well as on the vertical temperature gradient through N^2). In this respect, GW breaking cannot necessarily be considered as a process close to thermodynamic equilibrium. Second, it is the square of the thermodynamic forces that generally occur in the dissipation (47) in the case of linearized phenomenological equations. Here, however, the dependence on $\hat{\omega}_j$ and $\hat{\mathbf{c}}_{g,j}$ is more complex.

5. Proof of concept

To get an idea of how the parameterization of GW breaking due to 3DSI acts, we will consider a relatively simple setup and apply a number of simplifications to the governing equations.

Parameterizations of subgrid-scale GWs frequently make the steady-state and the columnar approximations. The former implies that the current of upward-propagating GWs adjusts instantaneously at each point of the vertical column to a changing upward inflow of GWs at the lower boundary of the column. In the columnar approximation, horizontal variations of the GW field and the resolved atmospheric state are neglected. Apart from this, direct interactions between the vertical momentum component and the GWs are ignored (e.g., Kim et al. 2003; Muraschko et al. 2015; Bölöni et al. 2016; Plougonven et al. 2020). If we apply these approximations to Eqs. (43e) and (43f), we find

$$\frac{\partial(\hat{c}_{gz,j}\mathcal{A}_j)}{\partial z} = \sigma_{\mathcal{A}_j}, \tag{56a}$$

$$\hat{c}_{gz,j}\frac{\partial \mathbf{k}_j}{\partial z} = -\left(\mathbf{e}_z \frac{\partial \mathbf{u}_0}{\partial z}\right)\cdot \mathbf{k}_{h,j} + \mathcal{A}_j^{-1}\boldsymbol{\sigma}_{\mathcal{P}_j}, \tag{56b}$$

where $\hat{c}_{gz} = -[(\hat{\omega}^2 - f^2)/\hat{\omega}]k_z/k^2$ is the vertical component of the intrinsic group velocity (without index j for brevity), and $\mathbf{u}_0$ denotes the horizontal part of the velocity $\mathbf{v}_0$. Then, according to Eqs. (43b) and (45) there is a vertical redistribution of momentum due to the GWs, which amounts to the following GW drag (e.g., Fritts and Alexander 2003; Kim et al. 2003; Bölöni et al. 2016):

$$\left.\frac{\partial \mathbf{u}_0}{\partial t}\right|_{\mathrm{GW}} = -\frac{1}{\rho}\frac{\partial}{\partial z}\left(\sum_{j=1}^{n}\hat{c}_{gz,j}\mathcal{A}_j\mathbf{k}_{h,j}\right). \tag{57}$$

In contrast to the form of the drag, there seems to be a broader range of approaches to the thermal effects associated with GW breaking (e.g., Becker and Schmitz 2002; Medvedev and Klaassen 2003; Becker 2004; Akmaev 2007). With the source of heat as its key element, the framework of irreversible thermodynamics automatically provides the form of the dissipative heating (when we speak of *heating* in the following, we always refer to the entropy budget, we do not refer to the budgets of internal energy or enthalpy). By combining Eqs. (30), (43d), and (47), we find for the dissipative GW heating rate in terms of the potential temperature:

$$\left.\frac{\partial \theta_0}{\partial t}\right|_{\mathrm{GW}} = \frac{\theta_0}{\rho_0 c_p T_0}\sum_{j=1}^{n}(\sigma_{\mathcal{A}_j}\hat{\omega}_j + \boldsymbol{\sigma}_{\mathcal{P}_j}\cdot\hat{\mathbf{c}}_{g,j}). \tag{58}$$

Whereas this heating is a direct effect of the irreversible GW breaking, the GW drag (57), itself reversible according to Eq. (45), is an indirect effect that follows from the destruction of wave action density. For purposes of comparison, we will also consider an alternative formulation of the GW heating rate, which is sometimes called the *frictional heating* associated with the GW drag (e.g., Becker and Schmitz 2002; Medvedev and Klaassen 2003; Walters et al. 2019):[10]

$$\left.\frac{\partial \theta_0}{\partial t}\right|_{\mathrm{GW}}^{(\mathrm{alt.})} = -\frac{1}{c_p \pi_0}\mathbf{u}_0 \cdot \left.\frac{\partial \mathbf{u}_0}{\partial t}\right|_{\mathrm{GW}}. \tag{59}$$

If we evaluate this alternative formulation from the viewpoint of the modeling approach presented in section 4, it is generally not in line with its requirements. In general, it cannot be guaranteed that this expression is positive definite. However, if different model assumptions are taken as a basis, Eq. (59) may be a consistent description of the thermal effects associated with GW breaking (see, e.g., Becker and Schmitz 2002; Medvedev and Klaassen 2003). Apart from that, Eq. (59) has the advantage over (58) that it provides a viable, cost-efficient way of closing the energy budget, without knowing details on the drag parameterization scheme. In addition, some schemes may provide a drag only, since it is not straightforward to

[9] However, this also depends on the quality criterion defined to measure the "adequacy" of the ansatz.

[10] We could arrive at this expression, if we neglect an explicit contribution of the GWs to the total energy budget (42), but retain the pseudomomentum flux in Eq. (45), this time, however, not as part of the reversible, but rather as part of the irreversible momentum flux. Then, the dissipation, (47), reads $T_0\sigma_s = \ldots - \hat{\mathbf{c}}_g\boldsymbol{\mathcal{P}}\cdot\cdot(\boldsymbol{\nabla}\mathbf{v}_0)^{\mathrm{T}} \approx \ldots + \mathbf{v}_0\cdot[\boldsymbol{\nabla}\cdot(\hat{\mathbf{c}}_g\boldsymbol{\mathcal{P}})] \approx \ldots - \rho_0\mathbf{u}_0\cdot(\partial\mathbf{u}_0/\partial t)_{\mathrm{GW}}$ [see Eq. (B2) in appendix B], where the first approximation requires $|\boldsymbol{\nabla}\cdot(\hat{\mathbf{c}}_g\boldsymbol{\mathcal{P}}\cdot\mathbf{v}_0)| \ll |\hat{\mathbf{c}}_g\boldsymbol{\mathcal{P}}\cdot\cdot(\boldsymbol{\nabla}\mathbf{v}_0)^{\mathrm{T}}|$ and the second approximation ignores $-\rho_0 w_0(\partial w_0/\partial t)_{\mathrm{GW}}$.

formulate a heating rate within the model framework on which they are based.

To solve Eqs. (56), we have to specify the spectrum of the GW inflow at the lower boundary of the vertical column. This boundary is called the launch level. For this purpose, we use the generalized Desaubies spectrum (e.g., Warner and McIntyre 2001; Scinocca 2003; McLandress and Scinocca 2005; MK19; Bölöni et al. 2021):

$$\mathcal{N}(k_z,\hat{\omega},\phi) = C\frac{|k_z/k_z^*|^s}{1+|k_z/k_z^*|^{s+t}}|\hat{\omega}/N|^{-(1+p)}, \tag{60}$$

where ϕ is the azimuth angle measured between the east direction and the horizontal part of the wave vector, C is a free parameter to scale the amount of wave action, and k_z^* denotes a characteristic vertical wavenumber. We need to take the absolute value of k_z, since upward-propagating GWs ($\hat{c}_{gz} > 0$) have $k_z < 0$ [see Eqs. (56)]. Taking the absolute value of $\hat{\omega}$ is for reasons of generality. We restrict our considerations to $\hat{\omega} > 0$, but that is not necessary. For the parameters, we use $k_z^* = 2\pi/2\,\mathrm{km}$, $s = 1$, $t = 3$ and $p = 3/2$ (see McLandress and Scinocca 2005; MK19). The spectrum (60) is commonly formulated in terms of the energy phase space density $\mathcal{E} = \mathcal{N}\hat{\omega}$ in the literature. It is a $[(k_z,\hat{\omega},\phi),\mathbf{x}]$-space density. To transform it into a $[(k_x,k_y,k_z),\mathbf{x}]$-space density, one can multiply with the Jacobian $\partial(k_z,\hat{\omega},\phi)/\partial(k_x,k_y,k_z) = (N^2-\hat{\omega}^2)/(\hat{\omega}k^2)$ (e.g., Warner and McIntyre 2001; Scinocca 2003; McLandress and Scinocca 2005; MK19; Bölöni et al. 2021). In the context of a discrete spectrum of GW packets, the continuous spectrum (60) can probably be interpreted and used in many different ways. For simplicity, we consider Eq. (60) as some kind of frequency distribution of GW packets in spectral space. Considering a spectral wave action element

$$\begin{aligned}\mathcal{N}(k_z,\hat{\omega},\phi)d\left|\frac{k_z}{k_z^*}\right|d\left|\frac{\hat{\omega}}{N}\right|d\phi &= C\underbrace{d\left[\frac{1}{2}\arctan\left(\left|\frac{k_z}{k_z^*}\right|^2\right)\right]}_{=:\chi}\\ &\quad\times\underbrace{d\left(-\frac{2}{3}\left|\frac{\hat{\omega}}{N}\right|^{-3/2}\right)}_{=:\xi}d\phi\\ &= Cd\chi d\xi d\phi,\end{aligned} \tag{61}$$

we find that the distribution is uniform in (χ, ξ, ϕ) space, where both relations $\chi(k_z)$ and $\xi(\hat{\omega})$ are monotonic in the range of interest. Therefore, we may take a given number of regularly distributed points in (χ, ξ, ϕ) space and map them to the corresponding points in (k_x, k_y, k_z) space, to roughly emulate the frequency distribution (cf. Scinocca 2003). The procedure is as follows: First, we will adopt a cylindrical coordinate system in spectral space, i.e., $(k_x, k_y, k_z) \to (k_h, k_z, \phi)$. Second, we specify a maximum horizontal wavelength $\lambda_{h,\max}$ and minimum and maximum vertical wavelengths $\lambda_{z,\min}$ and $\lambda_{z,\max}$ to compute the corresponding wavenumbers $k_{h,\min}(\lambda_{h,\max})$, $k_{z,\min}(\lambda_{z,\max})$, and $k_{z,\max}(\lambda_{z,\min})$. The squared intrinsic frequency may be written $\hat{\omega}^2 = N^2\cos^2\vartheta + f^2\sin^2\vartheta$, where ϑ denotes the altitude angle measured between the horizontal plane and $\mathbf{k}$. Then, we define $\hat{\omega}_{\min} := \hat{\omega}(k_{h,\min}, k_{z,\min})$ and $\hat{\omega}_{\mathrm{med}} := \hat{\omega}(\vartheta = 45°)$, where the latter is the intrinsic frequency of GWs with horizontal and vertical wavelengths of equal size. Now, we fix $\hat{\omega}_{\max}$ through the relation $(\hat{\omega}_{\max} - \hat{\omega}_{\mathrm{med}})/(\hat{\omega}_{\max} - \hat{\omega}_{\min}) = 0.1$, i.e., we arbitrarily choose the $\hat{\omega}$ range, where GWs have larger vertical than horizontal wavelengths to constitute 10% of the overall covered $\hat{\omega}$ range. Next, we specify the number of points in each coordinate direction, i.e., $\sum_{j=1}^{n} \to \sum_{j_h=1,j_z=1,j_\phi=1}^{n_h,n_z,n_\phi}$, with $n = n_h \times n_z \times n_\phi$ [see Eq. (36)]. With this, we can span a regular mesh in (χ, ξ, ϕ) space, with constant intervals $[\chi_{\max}(k_{z,\max}) - \chi_{\min}(k_{z,\min})]/(n_z - 1)$, $[\xi_{\max}(\hat{\omega}_{z,\max}) - \xi_{\min}(\hat{\omega}_{z,\min})]/(n_h - 1)$ and $360°/n_\phi$. Mapping back these points, we can assign to the GW packet indexed (j_h, j_z, j_ϕ) the properties $k_h[\hat{\omega}(\xi_{j_h}), k_z(\chi_{j_z})]$, $k_z(\chi_{j_z})$, and ϕ_{j_ϕ}. The points $(k_{h,j_hj_z}, k_{z,j_z}, \phi_{j_\phi})$ are then irregularly distributed according to Eq. (60) interpreted as frequency distribution. Each GW packet is assigned the same wave action density $\mathcal{A}_l$, which is fixed by prescribing the total pseudomomentum flux density F_l launched per azimuth, i.e., $\mathcal{A}_l\sum_j^n|\hat{c}_{gz,j}k_{h,j}|_{z=z_l} = n_\phi F_l$, where z_l denotes the vertical launch level [cf. Eq. (57)]. A steady upward current of GW packets with the above properties forms the lower boundary condition. We can then integrate Eqs. (56), for which we use a relatively simple finite-difference discretization. If one of the n vertical GW currents reaches a critical level (where the vertical wavelength vanishes), or experiences back-reflection (where the vertical group velocity becomes negative), the vertical integration is stopped and the wave action density is set to zero above.

Our testing consists in computing offline drag and heating rates for fixed atmospheric state profiles. Online tests with a general circulation model are not part of this work. We use the same profiles as MK19. These are representative zonal averages of zonal wind and temperature at 50° south for summer (January) and winter (June) from CIRA data (Fleming et al. 1990); see Fig. 3 (and Fig. 2 of MK19). For further parameters of the setup, we also closely follow MK19. We use $n_\phi = 2$ azimuths (i.e., east and west directions), a launch level of $z_l = 17$ km and a launch flux density per azimuth of $F_l = 7.2 \times 10^{-4}$ Pa. Apart from that, we set $n_h = n_z = 100$, $\lambda_{h,\max} = 50$ km, $\lambda_{z,\min} = 100$ m, $\lambda_{z,\max} = 20$ km, and $K_\epsilon = K_\zeta = 1$, $m = 5$ for the parameters of Eqs. (55). The layer thickness of the vertical grid is 1 km.

The wave action density at launch level $\mathcal{A}_l$ tends to decrease with increasing number of GW packets n (F_l held constant). If we would follow the ansatz that each GW breaks as if the other $(n - 1)$ were not present (see section 4f), the strength of the breaking, as described by Eqs. (55), would also depend significantly on n and tend to decrease with increasing n. The coefficients K_ϵ and K_ζ could be used to partially compensate for this effect, if desired. Here, however, we prefer to stay with $K_\epsilon = K_\zeta = 1$. Another possibility to reduce the dependence on n is to assume that the breaking is controlled by the superposition of all GWs, where Eq. (53) can be used to compute a collective instability time scale. The above discrete spectrum shows no variation in meridional direction ($k_y = 0$), since we use $n_\phi = 2$. As a result, the coefficient c vanishes and the characteristic Eq. (9) is reduced to a quadratic equation again.

For purposes of comparison, we also compute the GW drag for the case that the GW breaking is assumed to be triggered

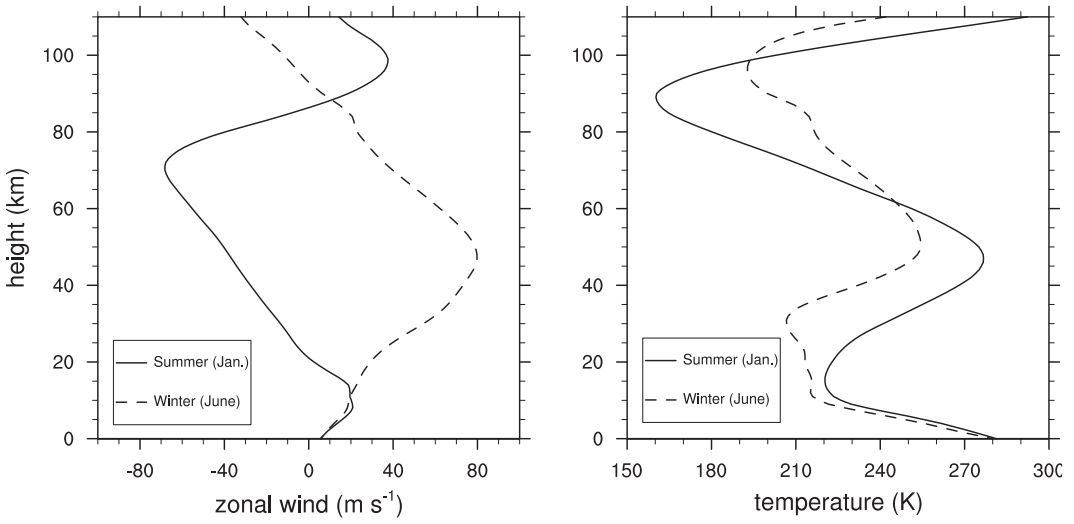

FIG. 3. Profiles of zonal averages of (left) zonal wind and (right) temperature at 50° south for summer (January, solid lines) and winter (June, dashed lines) from CIRA data.

by VSI instead of 3DSI. To achieve this, we set each component of the deviation stability tensor $\mathbf{S}'$ [see Eq. (53)], except for S'_{zz}, to zero. In the following comparison to the results of MK19, however, we always refer to the results of the full 3DSI scheme.

Before testing the full CIRA profiles, we apply the scheme to the summer temperature profile plus zero zonal wind ($u_0 = 0$ m s^{-1}). East- and westward GW drag profiles for this case are shown in Fig. 4 (left panel, blue solid lines). They cancel each other exactly, due to the azimuthal symmetry of the wind profile and the launched GW spectrum. The total GW heating rate profiles according to Eqs. (58) and (59) are shown in Fig. 5. The dissipative heating, (58), is accumulative and does not vanish. The alternative frictional heating, (59), is zero in this (admittedly highly idealized) case. The drag profiles can be compared to Fig. 5 of MK19, where the authors show GW drag profiles for the Hines (1997) scheme, on the one hand, and for the Warner and McIntyre (2001) and Scinocca (2003) scheme (WMS, hereafter), on the other hand. In contrast to the present scheme, which is based on a discrete spectrum of GW packets, the Hines and WMS schemes are based on a continuous GW spectrum. Apart from that, the latter two schemes differ in many respects from each other (see the aforementioned literature for more details). The drag profiles in Fig. 4 (left panel) are more similar to the WMS than to the Hines drag profiles, both in shape and in magnitude. The Hines profiles exhibit an oscillatory structure and are about 10 times larger in magnitude.

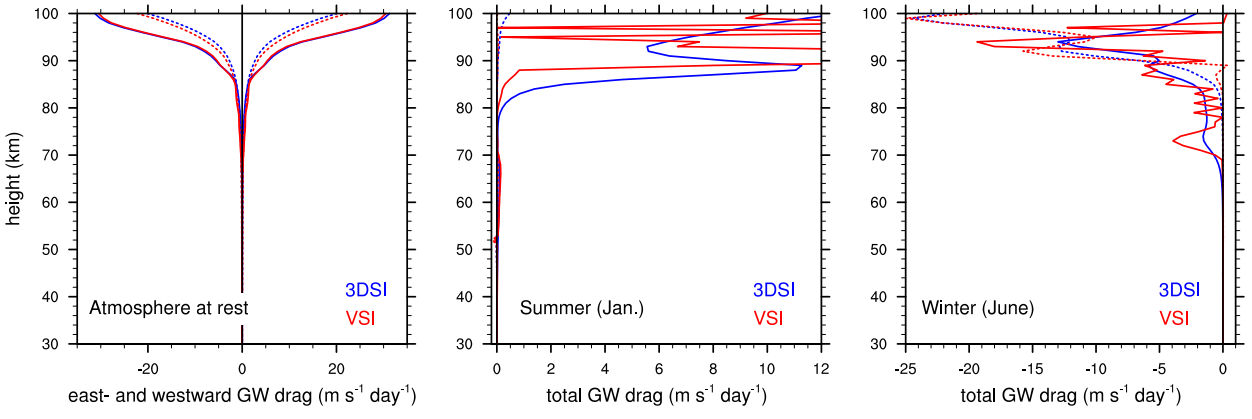

FIG. 4. (left) Vertical GW drag profiles for an atmosphere at rest, and the CIRA zonal wind and temperature profiles, shown in Fig. 3, for (center) summer and (right) winter. In the left panel eastward (positive) and westward (negative) GW drag profiles are plotted separately. The center and right panels show the total GW drag (east- plus westward drag). Results for the three-dimensional static instability (3DSI) and vertical static instability (VSI) are shown in blue and red, respectively. Solid lines represent the case $K_\epsilon = K_\zeta = 1$, dotted lines represent the case $K_\epsilon = 1$, $K_\zeta = 0$. Drag magnitudes below 30 km are comparatively small and therefore not plotted. The red solid line in the middle panel peaks at 25 m s^{-1} day^{-1}, but we cut at 12 m s^{-1} day^{-1} to show the other lines more clearly.

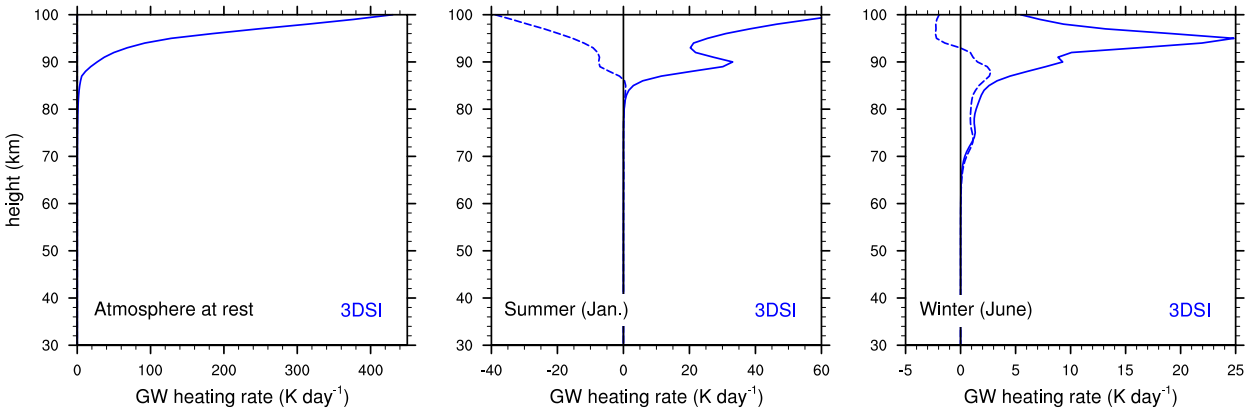

FIG. 5. Vertical profiles of the total GW heating rates corresponding to the GW drag profiles in Fig. 4. Solid lines are heating rates according to Eq. (58), dashed lines according to Eq. (59).

Vertical profiles of the total (east- plus westward) GW drag for the full CIRA profiles are shown in Fig. 4 (middle and right panels, blue solid lines). They can be compared to Fig. 6 of MK19, where corresponding profiles for the Hines and the WMS schemes are shown. Both schemes yield predominantly westward drag in the winter case and predominantly eastward drag in the summer case. The results shown in Fig. 4 are in line with this characteristic. In terms of the shape of the drag profile, the WMS scheme produces a relatively smooth profile, with drag spread over a broad altitude range. In contrast, the Hines scheme produces a relatively localized forcing of a rather oscillatory shape (see MK19 for a detailed analysis). The drag profiles in Fig. 4 lie in between. The shape is significantly less smooth than in case of the WMS scheme, but not as erratic as in case of the Hines scheme. The strength of the drag in both cases is comparable to what the WMS scheme produces. The drag of the Hines scheme is about two orders of magnitude stronger than the WMS drag. A number of discrepancies between the Hines and WMS schemes, on the one hand, and the present scheme, on the other hand, might have two main reasons. First, a continuous GW spectrum forms the (theoretical) basis of their schemes, whereas we use a discrete spectrum. Second, the present scheme describes the GW dissipation by explicit sinks in the GW budget equations, (56), whereas the other two schemes use an "instantaneous" adjustment to a saturation or reference spectrum, in one form or another. Future investigations have to reveal the specific reasons.

The drag based on VSI is of comparable magnitude as the 3DSI drag, in particular in the atmosphere-at-rest case. This is mainly due to the azimuthal symmetry of the discrete spectrum. For even n_ϕ, the off-diagonal components of $\mathbf{S}'$ vanish, since the contributions of different GW packets cancel each other. As a result, the root of Eq. (9) that is associated with the (most) unstable mode differs only slightly between 3DSI and VSI. In the summer and winter cases, where the wind breaks the symmetry, differences are more pronounced. The VSI drag is significantly more oscillatory than the 3DSI drag. This can be attributed in large part to the pseudomomentum source [see Eq. (55b)], as computations with $K_\zeta = 0$ reveal (see Fig. 4, dotted lines). The winter case shows this more clearly, as the drag magnitude becomes relatively small for $K_\zeta = 0$ in the summer case. The vertical component of the source tends to increase the vertical wavenumber k_z. This in turn can amplify the VSI (cf. Fig. 1, right panel). The instability can become so strong that the relaxation of the wave action according to Eq. (55a) results in a statically stable configuration of the spectrum, whereupon the strength of the sources (55) drops to zero. Then the cycle repeats, since the upward propagation restores the instability. For 3DSI, the process is comparable, but there are at least two differences, which may result in a smoother drag profile. First, the area of instability in $\mathbf{k}$ space is significantly larger for 3DSI than for VSI (see Fig. 1). As a consequence, abrupt changes between unstable and stable spectral configurations are less likely. Second, the horizontal component of the pseudomomentum source (55b) tends to decrease the horizontal wavenumber k_h. This can reduce the strength of 3DSI in certain areas of $\mathbf{k}$ space (see Fig. 1, middle panel).

Heating rates according to Eqs. (58) and (59) are shown in Fig. 5 (middle and right panels), but only for 3DSI. The dissipative heating (58) and the frictional heating (59) are of comparable magnitude, at least at altitudes above about 70 km. Whereas the dissipative heating is exclusively positive, there are altitude ranges, where the frictional heating would cool the atmosphere. If the frictional heating would be used as a model for dissipative heating, this would be an undesirable behavior. Here, however, we can only speak for the present scheme. If the drag is in opposite direction to the wind, the frictional heating is positive, and this seems to be the case for a broad altitude range for both the Hines and the WMS schemes (cf. Figs. 2 and 6 of MK19). The magnitude of the heating rate profiles for the summer and winter cases is comparable to heating rates presented by Medvedev and Klaassen (2003) and Becker (2004).

The aim of this proof of concept was to give an idea of the characteristics of the present scheme. In summary, it can produce drag profiles that are similar to the profiles of the WMS scheme, both in shape and in magnitude. Using 3DSI instead of VSI can make a difference for the drag. In general, the

3DSI profiles are smoother than the VSI profiles. Future studies, in which the present scheme is implemented in a general circulation model, have to reveal, if the present scheme can compete with established schemes.

In terms of computational costs, a parameterization scheme based on a discrete spectrum of GWs that attempts to be in line with the principles of irreversible thermodynamics, can likely not compete with established schemes such as the Hines and WMS schemes. The WMS scheme, for instance, is based on the continuous spectrum, (60), and through an analytical integration over the $\hat{\omega}$ dependence, it is able to reduce the problem to 2D in spectral space. In addition, these schemes do not consider explicit irreversible sources and fluxes in the GW budget equations, but rather apply an "instantaneous" adjustment to a saturation spectrum, in one form or another, which is generally less expensive. Nevertheless, the scheme presented here could become feasible in atmospheric models with a relatively high grid resolution, where the major part of the GW spectrum is already explicitly resolved, and only a relatively small part of it remains to be parameterized. Alternatively, the scheme might be employed for stochastic parameterizations, where only a few GW packets (or rather GW packet currents) are launched per column, whose properties vary in space and time (e.g., Eckermann 2011).

Finally, there is another aspect of GW parameterizations pointed out, for instance, by Amemiya and Sato (2016) and MK19. Although shape and strength of the GW drag may be quite different for two GW schemes under the same atmospheric conditions, the response of a general circulation model to them may be relatively similar. The resolved model atmosphere appears to show the tendency of compensating different forcings. So two different schemes may result in similar wind statistics. This adjustment effect concerns at least momentum tendencies, which can cancel each other. Dissipative heating, in contrast, is accumulative. What this means in terms of the response behavior of a general circulation model is probably less clear than in case of the GW drag.

6. Summary

Vertical static instability (VSI) is a common indicator for the onset of gravity wave (GW) breaking in the atmosphere, according to which instability sets in, if the vertical gradient of potential temperature of the atmospheric state modulated by the presence of a GW becomes negative. Horizontal variations, whose magnitude can be significant for nonhydrostatic GWs, are ignored in this analysis. Hines (1971, 1988) proposed an alternative approach that accounts for horizontal variations and he found that this analysis predicts an unconditional instability, if GWs are present. This instability is called slantwise static instability (SSI). Some aspects of the analysis method of Hines make, however, the use of its results in certain areas of application difficult, for instance, in a parameterization of the GW breaking that could be triggered by the instability. In this work, we show that the method of Godson (1950) and Shutts and Cullen (1987) may be an alternative. It is related to the method of Hines, and similar to SSI, it predicts a significantly larger range of instability than VSI. We call this instability 3DSI to distinguish it from SSI. In terms of their mathematical expressions, it appears more straightforward to incorporate 3DSI into the development of a parameterization than SSI. We use this fact to make a suggestion for such a parameterization.

To meet the irreversible character of the process of GW breaking, we apply the methods of irreversible thermodynamics, which are embedded in the Gibbs formalism of dynamics. In this way, the parameterization does not only satisfy the second law of thermodynamics, but it can also be made consistent with the conservation of energy and further (non-)conservation principles, if required. In addition to an expression for the GW drag, we obtain an expression for the heating rate associated with the GW breaking, since the production of entropy is at the heart of the approach.

We develop the parameterization for a discrete spectrum of GWs. Following general practice, we apply the steady-state and columnar approximations. Offline computations of GW drag and heating rates are performed for two vertical zonal wind and temperature profiles from CIRA data. One profile is representative for summer, the other for winter conditions. The same profiles where use by MK19 to analyze the GW drag from the Hines (1997) scheme, on the one hand, and the WMS scheme, on the other hand. So our results can be compared with their findings. The GW drag produced by the present scheme is less smooth than the drag produced by the WMS scheme, but still less oscillatory than the drag from the Hines scheme. For both the summer and winter cases the strength of the drag is comparable to the result of the WMS scheme, but significantly less than the result of the Hines scheme. In addition, we show that replacing 3DSI by VSI in the present scheme can change the drag significantly. Although the strength of the drag is of the same magnitude in both cases, the 3DSI drag profiles are significantly smoother than the VSI drag profiles. The dissipative heating rate produced by the present scheme is always positive and in line with the second law of thermodynamics. It is shown that the frictional heating, which follows directly from the GW drag, is not necessarily positive and should be used with care in the case that it is employed for the parameterization of dissipative heating. Future investigations with the present scheme implemented in a general circulation model have to show whether it can compete with established schemes.

Acknowledgments. The authors thank the German Research Foundation (DFG) for partial support through the research unit Multiscale Dynamics of Gravity Waves (MS-GWaves) and through Grant ZA 268/10-2. We greatly appreciate many helpful discussions with Dr. Young-Ha Kim and Dr. Gergely Bölöni. Their valuable suggestions led to significant improvements of the manuscript. We are indebted to the anonymous reviewers for very helpful comments.

Data availability statement. The scripts and the source code that were used to produce the results, which are shown in the figures of this work, can be made available upon request. Please contact the corresponding author.

APPENDIX A

The Determinant of a Tensor

Here, we state the determinant of a second-order tensor of the form $\mathbf{D} = \alpha\mathbf{I} + \beta\mathbf{W} + \gamma\mathbf{S}$, where α, β, and γ are scalar coefficients (arbitrary for the time being), and $\mathbf{I}$, $\mathbf{W}$, and $\mathbf{S}$ are the identity, angular velocity, and stability tensors, respectively. All that is necessary to derive the determinant can be found, e.g., in Wilson (1929), Sihvola (1999), Viúdez (2005), Zdunkowski and Bott (2003), and Lebedev et al. (2010). The derivation is relatively lengthy and beyond the scope of this work. We just state the final result.

We need two tensor products in order to express the determinant. First, the double scalar product (or double-dot product)

$$\begin{aligned}\mathbf{A}\cdot\cdot\mathbf{B} &:= (A_{ij}\mathbf{e}_i\mathbf{e}_j)\cdot\cdot(B_{kl}\mathbf{e}_k\mathbf{e}_l) = A_{ij}B_{kl}\mathbf{e}_i\mathbf{e}_j\cdot\cdot\mathbf{e}_k\mathbf{e}_l\\ &= A_{ij}B_{kl}(\mathbf{e}_i\mathbf{e}_j\cdot\mathbf{e}_k)\cdot\mathbf{e}_l = A_{ij}B_{kl}(\mathbf{e}_j\cdot\mathbf{e}_k)(\mathbf{e}_i\cdot\mathbf{e}_l) = A_{ij}B_{ji},\end{aligned} \tag{A1}$$

where $\mathbf{e}_i,\ldots,\mathbf{e}_l$ denote unit vectors of an arbitrary normal basis, and $A_{ij}\mathbf{e}_i\mathbf{e}_j$, for instance, is an abbreviation for $\sum_{i,j=1}^{3}A_{ij}\mathbf{e}_i\mathbf{e}_j$. The result of the product (A1) is a scalar. From Eq. (A1) the following identities may be derived: $\mathbf{A}\cdot\cdot\mathbf{B} = \mathbf{B}\cdot\cdot\mathbf{A} = \mathbf{A}^{\mathrm{T}}\cdot\cdot\mathbf{B}^{\mathrm{T}} = \mathbf{B}^{\mathrm{T}}\cdot\cdot\mathbf{A}^{\mathrm{T}}$, and $\mathbf{a}\cdot\mathbf{b} = (\mathbf{I}\cdot\mathbf{a})\cdot\mathbf{b} = \mathbf{I}\cdot\cdot\mathbf{ab} = \mathbf{ab}\cdot\cdot\mathbf{I} = \mathbf{I}^{\mathrm{T}}\cdot\cdot(\mathbf{ab})^{\mathrm{T}} = \mathbf{I}\cdot\cdot\mathbf{ba} = \mathbf{ba}\cdot\cdot\mathbf{I}$, where $\mathbf{I}^{\mathrm{T}} = \mathbf{I}$ was used. Second, we need the double cross product:

$$\mathbf{A}\times\times\mathbf{B} := A_{ij}B_{kl}\mathbf{e}_i\mathbf{e}_j\times\times\mathbf{e}_k\mathbf{e}_l = A_{ij}B_{kl}(\mathbf{e}_j\times\mathbf{e}_k)(\mathbf{e}_i\times\mathbf{e}_l). \tag{A2}$$

Like its two factors, the product (A2) is a second-order tensor. From Eq. (A2) the following identities may be derived: $\mathbf{A}\times\times\mathbf{B} = \mathbf{B}^{\mathrm{T}}\times\times\mathbf{A}^{\mathrm{T}} = (\mathbf{B}\times\times\mathbf{A})^{\mathrm{T}}$. With this, the determinant of a tensor $\mathbf{A}$ reads

$$\det(\mathbf{A}) := \frac{1}{3}\mathrm{adj}(\mathbf{A})\cdot\cdot\mathbf{A} = \frac{1}{6}(\mathbf{A}\times\times\mathbf{A}^{\mathrm{T}})\cdot\cdot\mathbf{A}, \tag{A3}$$

where $\mathrm{adj}(\mathbf{A}) = (\mathbf{A}\times\times\mathbf{A}^{\mathrm{T}})/2$ denotes the adjugate of $\mathbf{A}$. Since the inverse of $\mathbf{A}$ can be expressed as $\mathbf{A}^{-1} = \mathrm{adj}(\mathbf{A})/\det(\mathbf{A})$, it follows that $\mathrm{adj}(\mathbf{A})\cdot\mathbf{A} = \det(\mathbf{A})\mathbf{I}$. It can be shown that the determinant of a tensor of the form $\mathbf{D}$ reads

$$\begin{aligned}\det(\mathbf{D}) = {}&\alpha^3 + \alpha^2\gamma\,\mathrm{tr}(\mathbf{S}) + \alpha\beta^2\Omega^2 + \alpha\gamma^2\frac{1}{2}[\mathrm{tr}^2(\mathbf{S}) - \mathbf{S}\cdot\cdot\mathbf{S}]\\ &+ \beta^2\gamma\boldsymbol{\Omega}\boldsymbol{\Omega}\cdot\cdot\mathbf{S} + \gamma^3\det(\mathbf{S}),\end{aligned} \tag{A4}$$

where $\mathrm{tr}(\mathbf{S}) := \mathbf{I}\cdot\cdot\mathbf{S}$ denotes the trace of $\mathbf{S}$, and $\mathrm{tr}^2(\mathbf{S}) := [\mathrm{tr}(\mathbf{S})]^2$. In addition, $\Omega^2 := \boldsymbol{\Omega}\cdot\boldsymbol{\Omega}$, where $\boldsymbol{\Omega}$ is the angular velocity vector ($\mathbf{W} = \boldsymbol{\Omega}\times\mathbf{I}$). For Eq. (A4) we used that $\det(\mathbf{I}) = 1$ and $\det(\mathbf{W}) = 0$, in addition to many more identities for which we have to refer to the literature cited above. With $\alpha = d^2/dt^2$, $\beta = 2d/dt$, and $\gamma = 1$, we find

$$\begin{aligned}\det(\mathbf{D}) = {}&\frac{d^6}{dt^6} + \underbrace{[\mathrm{tr}(\mathbf{S}) + 4\Omega^2]}_{=:a}\frac{d^4}{dt^4}\\ &+ \underbrace{\left\{\frac{1}{2}[\mathrm{tr}^2(\mathbf{S}) - \mathbf{S}\cdot\cdot\mathbf{S}] + 4\boldsymbol{\Omega}\boldsymbol{\Omega}\cdot\cdot\mathbf{S}\right\}}_{=:b}\frac{d^2}{dt^2} + \underbrace{\det(\mathbf{S})}_{=:c},\end{aligned} \tag{A5}$$

where $\mathbf{I}$, $\mathbf{W}$, and $\mathbf{S}$ are constant.

Finally, we consider how the above quantities can be computed in a Cartesian coordinate system on an f plane tangential to the mean sea level surface of Earth at the geographical position (λ_0, φ_0), with zonal, meridional, and vertical unit vectors $\mathbf{e}_x$, $\mathbf{e}_y$, and $\mathbf{e}_z$. If we measure $\mathbf{S}$ in Cartesian coordinates and arrange the coefficients of this measurement in a matrix denoted by $(\mathbf{S})_{\mathrm{cc}}$, we find

$$\begin{aligned}(\mathbf{S})_{\mathrm{cc}} &= \begin{pmatrix}S_{xx} & S_{xy} & S_{xz}\\ S_{yx} & S_{yy} & S_{yz}\\ S_{zx} & S_{zy} & S_{zz}\end{pmatrix} = \begin{pmatrix}S_{xx} & S_{xy} & S_{xz}\\ S_{xy} & S_{yy} & S_{yz}\\ S_{xz} & S_{yz} & S_{zz}\end{pmatrix}\\ &= c_p\theta\begin{pmatrix}\frac{\partial^2\pi}{\partial x^2} & \frac{\partial^2\pi}{\partial x\partial y} & \frac{\partial^2\pi}{\partial x\partial z}\\ \frac{\partial^2\pi}{\partial x\partial y} & \frac{\partial^2\pi}{\partial y^2} & \frac{\partial^2\pi}{\partial y\partial z}\\ \frac{\partial^2\pi}{\partial x\partial z} & \frac{\partial^2\pi}{\partial y\partial z} & \frac{\partial^2\pi}{\partial z^2}\end{pmatrix},\end{aligned} \tag{A6}$$

where we used the symmetry of $\mathbf{S}$ and $\boldsymbol{\nabla}\Phi = \text{const.}$, so that $\boldsymbol{\nabla}\boldsymbol{\nabla}\Phi = 0$ (see section 2). Just for completeness, we add expressions for the tensors $\mathbf{I}$, $\mathbf{W} = \boldsymbol{\Omega}\times\mathbf{I}$ and $\mathrm{adj}(\mathbf{S})$, and the dyad $\boldsymbol{\Omega}\boldsymbol{\Omega}$

$$\begin{aligned}(\mathbf{I})_{\mathrm{cc}} &= \begin{pmatrix}1 & 0 & 0\\ 0 & 1 & 0\\ 0 & 0 & 1\end{pmatrix},\quad (\mathbf{W})_{\mathrm{cc}} = \frac{f}{2}\begin{pmatrix}0 & -1 & 0\\ 1 & 0 & 0\\ 0 & 0 & 0\end{pmatrix},\\ (\boldsymbol{\Omega}\boldsymbol{\Omega})_{\mathrm{cc}} &= \frac{f^2}{4}\begin{pmatrix}0 & 0 & 0\\ 0 & 0 & 0\\ 0 & 0 & 1\end{pmatrix},\\ [\mathrm{adj}(\mathbf{S})]_{\mathrm{cc}} &= \begin{pmatrix}S_{yy}S_{zz} - S_{yz}^2 & S_{xz}S_{yz} - S_{xy}S_{zz} & S_{xy}S_{yz} - S_{xz}S_{yy}\\ S_{xz}S_{yz} - S_{xy}S_{zz} & S_{xx}S_{zz} - S_{xz}^2 & S_{xy}S_{xz} - S_{xx}S_{yz}\\ S_{xy}S_{yz} - S_{xz}S_{yy} & S_{xy}S_{xz} - S_{xx}S_{yz} & S_{xx}S_{yy} - S_{xy}^2\end{pmatrix},\end{aligned} \tag{A7}$$

where we used that $(2\boldsymbol{\Omega})_{\mathrm{cc}} = (0, 0, 2\Omega\sin\varphi_0) =: (0, 0, f)$. In addition, the coefficients a, b, and c of Eq. (A5) read

$$a = S_{xx} + S_{yy} + S_{zz} + f^2, \tag{A8a}$$

$$b = S_{xx}S_{yy} - S_{xy}^2 + S_{xx}S_{zz} - S_{xz}^2 + S_{yy}S_{zz} - S_{yz}^2 + f^2S_{zz}, \tag{A8b}$$

$$\begin{aligned}c = {}&S_{xx}(S_{yy}S_{zz} - S_{yz}^2) - S_{xy}(S_{xy}S_{zz} - S_{yz}S_{xz})\\ &+ S_{xz}(S_{xy}S_{yz} - S_{yy}S_{xz}).\end{aligned} \tag{A8c}$$

APPENDIX B

Divergence of the Product of a Tensor and a Vector

Following Wilson (1929), Sihvola (1999), Zdunkowski and Bott (2003), and Lebedev et al. (2010), we may write

$$\nabla\cdot(\mathbf{A}\cdot\mathbf{c}) = \nabla\cdot(\overset{\downarrow}{\mathbf{A}}\cdot\mathbf{c}) + \nabla\cdot(\mathbf{A}\cdot\overset{\downarrow}{\mathbf{c}}) = (\nabla\cdot\mathbf{A})\cdot\mathbf{c} + (\mathbf{A}^{\mathrm{T}}\cdot\nabla)\cdot\mathbf{c}$$
$$= \mathbf{c}\cdot(\nabla\cdot\mathbf{A}) + \mathbf{A}^{\mathrm{T}}\cdot\cdot\nabla\mathbf{c} = \mathbf{c}\cdot(\nabla\cdot\mathbf{A}) + \mathbf{A}\cdot\cdot(\nabla\mathbf{c})^{\mathrm{T}}, \tag{B1}$$

where the arrow ↓ indicates the quantity, the derivative acts on, and Eq. (A1) was used in the last steps. Replacing the tensor $\mathbf{A}$ by a dyad $\mathbf{ab}$ then yields

$$\nabla\cdot(\mathbf{ab}\cdot\mathbf{c}) = \mathbf{c}\cdot[\nabla\cdot(\mathbf{ab})] + (\mathbf{ab})^{\mathrm{T}}\cdot\cdot\nabla\mathbf{c}$$
$$= \mathbf{c}\cdot[\nabla\cdot(\mathbf{ab})] + \mathbf{ba}\cdot\cdot\nabla\mathbf{c}. \tag{B2}$$

APPENDIX C

Expansion of a Second-Order Tensor in Deviatoric, Spherical, and Skew-Symmetric Parts

First, an arbitrary tensor $\mathbf{A}$ may be divided into symmetric and skew-symmetric parts (e.g., Herbert 1978; Jou et al. 2001; Zdunkowski and Bott 2003, 2004; Papenfuß 2020):

$$\mathbf{A} = \underbrace{\frac{1}{2}(\mathbf{A}+\mathbf{A}^{\mathrm{T}})}_{=:\mathrm{sym}(\mathbf{A})} + \underbrace{\frac{1}{2}(\mathbf{A}-\mathbf{A}^{\mathrm{T}})}_{=:\mathrm{skw}(\mathbf{A})}, \tag{C1}$$

with $\mathrm{sym}(\mathbf{A})^{\mathrm{T}} = \mathrm{sym}(\mathbf{A})$ and $\mathrm{skw}(\mathbf{A})^{\mathrm{T}} = -\mathrm{skw}(\mathbf{A})$. The symmetric part, in turn, may be divided into deviatoric and spherical (or isotropic) parts:

$$\mathrm{sym}(\mathbf{A}) = \underbrace{\frac{1}{2}\left(\mathbf{A}+\mathbf{A}^{\mathrm{T}}-\frac{2}{3}\mathrm{tr}(\mathbf{A})\mathbf{I}\right)}_{=:\mathrm{dev}(\mathbf{A})} + \underbrace{\frac{\mathrm{tr}(\mathbf{A})}{3}\mathbf{I}}_{=:\mathrm{sph}(\mathbf{A})}, \tag{C2}$$

where tr() denotes the trace of a tensor, a scalar quantity, and $\mathbf{I}$ is the identity tensor. Both deviatoric and spherical parts are symmetric, too. The deviatoric part is traceless $\mathrm{tr}[\mathrm{dev}(\mathbf{A})] = 0$, and the trace of the spherical part reads $\mathrm{tr}[\mathrm{sph}(\mathbf{A})] = [\mathrm{tr}(\mathbf{A})/3]\mathrm{tr}(\mathbf{I}) = \mathrm{tr}(\mathbf{A})$, since $\mathrm{tr}(\mathbf{I}) = 3$. These three parts are orthogonal with respect to the double scalar product [see Eq. (A1)]:

$$\mathbf{A}\cdot\cdot\mathbf{B} = \mathrm{dev}(\mathbf{A})\cdot\cdot\mathrm{dev}(\mathbf{B}) + \mathrm{sph}(\mathbf{A})\cdot\cdot\mathrm{sph}(\mathbf{B}) + \mathrm{skw}(\mathbf{A})\cdot\cdot\mathrm{skw}(\mathbf{B}), \tag{C3}$$

where $\mathbf{B}$ is another arbitrary tensor.

APPENDIX D

List of Symbols

t, $\mathbf{x}$	Time and position vector
x, y, z	Zonal (west–east), meridional (south–north), and vertical (bottom-up) components of position
$\mathbf{e}_x$, $\mathbf{e}_y$, $\mathbf{e}_z$	Unit vectors in zonal, meridional, and vertical directions
d/dt, $\partial/\partial t$	Lagrangian (or material) and Eulerian time derivatives
$\nabla = \partial/\partial\mathbf{x}$	Nabla operator
$\nabla\nabla = \partial^2/\partial\mathbf{x}\partial\mathbf{x}$	Second-order Hessian tensor
$\mathbf{I}$	Second-order identity tensor
Φ	Potential of apparent gravity (true gravity plus centrifugal acceleration)
$\mathbf{g} = g\mathbf{e}_z$	Mean gravitational acceleration at sea level
$\boldsymbol{\Omega}$, $\mathbf{W} = \boldsymbol{\Omega}\times\mathbf{I}$	Vector and second-order tensor of Earth's angular velocity
c_p, c_v, R	Specific heat capacities at constant pressure and at constant volume, gas constant of dry air
T, p, ρ, θ, π, $\mathbf{v}$	Temperature, pressure, density, potential temperature, Exner pressure, and velocity (or wind) vector
$\mathbf{u}$, u, v, w	Horizontal part of the velocity vector $\mathbf{v}$, and zonal, meridional, and vertical components of $\mathbf{v}$
$\delta(\cdot)$	Difference of a quantity between perturbed and unperturbed air parcel
$\mathbf{S}$	Second-order stability tensor
$\overline{N}^2$, N^2	Squared buoyancy and Brunt–Väisälä frequencies
$f = 2\Omega\sin(\varphi)$	Coriolis parameter at latitude φ
$(\cdot)_{00}$	Constant reference value of a quantity
$(\cdot)_0$	Hydrostatic, atmospheric background state or resolved (gridscale) quantities, respectively
$(\cdot)'$	Perturbation of a quantity associated with a GW, or unresolved (subgrid-scale) quantity, respectively
i, $\mathrm{Re}\{\cdot\}$, $\mathrm{Im}\{\cdot\}$	Imaginary unit, real, and complex parts of a complex quantity
$\widehat{(\cdot)}$	Complex oscillation or wave amplitude quantity
$\overline{\omega}$	Oscillation frequency of a perturbed (displaced) parcel
a, b, c	Coefficients of the characteristic equation for $\overline{\omega}$
$\mathbf{k}$, $\nabla_{\mathbf{k}} = \partial/\partial\mathbf{x}$	Wave vector and derivative with respect to the same
k_x, k_y, k_z	Zonal, meridional, and vertical components of wave vector
λ_h, λ_z	Horizontal and vertical wavelength
ω, $\hat{\omega}$	Extrinsic and intrinsic GW frequencies
$\mathbf{N}^2$	Second-order GW dispersion relation tensor
$\mathbf{c}_g$, $\hat{\mathbf{c}}_g$	Extrinsic and intrinsic GW group velocities
$\mathcal{T}_{\mathrm{GW}}$, $\mathcal{T}_{\mathrm{in}}$, τ	Intrinsic GW period, time scale of instability, and $\mathcal{T}_{\mathrm{GW}}$-to-$\mathcal{T}_{\mathrm{in}}$ ratio
E, m, $\mathbf{P}$, V, S	Energy, mass, momentum, volume, and entropy
e, $\mathbf{p}$, v, s	Mass-specific energy, momentum, volume, and entropy
$\tilde{e}'$, $\mathcal{A}$, $\mathcal{P}$	Energy, wave action, and pseudomomentum densities of a (unresolved) GW packet
$\mathcal{N}$	Wave action phase space density
$\mathbf{x}_g$, d_g/dt	Position of a GW packet and GW packet–fixed time derivative
$\overset{r}{\mathbf{F}}$, $\overset{r}{\mathbf{F}}$	Vectorial and tensorial densities of reversible fluxes
$\overset{i}{\mathbf{F}}$, $\overset{i}{\mathbf{F}}$	Vectorial and tensorial densities of irreversible fluxes
σ, $\boldsymbol{\sigma}$	Scalar and vectorial densities of irreversible sources

L, $\mathbf{L}$, L, $\mathbf{L}^{(3)}$, $\mathbf{L}^{(4)}$	Scalar, vectorial, second-, third-, and fourth-order tensorial transport coefficients of linearized phenomenological equations
$(\cdot)^{\mathrm{T}}$, adj$(\cdot)$, det$(\cdot)$, tr$(\cdot)$	Transpose, adjugate, determinant, and trace of a second-order tensor
sym$(\cdot)$, skw$(\cdot)$, dev$(\cdot)$, sph$(\cdot)$	Symmetric, skew-symmetric, deviatoric, and spherical (or isotropic) parts of a second-order tensor
$(\cdot)\cdot\cdot(\cdot)$	Double scalar product of two tensors
i, j, k, l, m	Indices

REFERENCES

Achatz, U., B. Ribstein, F. Senf, and R. Klein, 2017: The interaction between synoptic-scale balanced flow and a finite-amplitude mesoscale wave field throughout all atmospheric layers: Weak and moderately strong stratification. *Quart. J. Roy. Meteor. Soc.*, **143**, 342–361, https://doi.org/10.1002/qj.2926.

Akmaev, R. A., 2007: On the energetics of mean-flow interactions with thermally dissipating gravity waves. *J. Geophys. Res.*, **112**, D11125, https://doi.org/10.1029/2006JD007908.

Alexander, M. J., and T. J. Dunkerton, 1999: A spectral parameterization of mean-flow forcing due to breaking gravity waves. *J. Atmos. Sci.*, **56**, 4167–4182, https://doi.org/10.1175/1520-0469(1999)056<4167:ASPOMF>2.0.CO;2.

Amemiya, A., and K. Sato, 2016: A new gravity wave parameterization including three-dimensional propagation. *J. Meteor. Soc. Japan*, **94**, 237–256, https://doi.org/10.2151/jmsj.2016-013.

Amiramjadi, M., A. R. Mohebalhojeh, M. Mirzaei, C. Zülicke, and R. Plougonven, 2020: The spatiotemporal variability of nonorographic gravity wave energy and relation to its source functions. *Mon. Wea. Rev.*, **148**, 4837–4857, https://doi.org/10.1175/MWR-D-20-0195.1.

Becker, E., 2004: Direct heating rates associated with gravity wave saturation. *J. Atmos. Sol.-Terr. Phys.*, **66**, 683–696, https://doi.org/10.1016/j.jastp.2004.01.019.

——, and G. Schmitz, 2002: Energy deposition and turbulent dissipation owing to gravity waves in the mesosphere. *J. Atmos. Sci.*, **59**, 54–68, https://doi.org/10.1175/1520-0469(2002)059<0054:EDATDO>2.0.CO;2.

Blackadar, A. K., 1955: Extension of the laws of thermodynamics to turbulent systems. *J. Atmos. Sci.*, **12**, 165–175, https://doi.org/10.1175/1520-0469(1955)012<0165:EOTLOT>2.0.CO;2.

Bölöni, G., B. Ribstein, J. Muraschko, C. Sgoff, J. Wei, and U. Achatz, 2016: The interaction between atmospheric gravity waves and large-scale flows: An efficient description beyond the nonacceleration paradigm. *J. Atmos. Sci.*, **73**, 4833–4852, https://doi.org/10.1175/JAS-D-16-0069.1.

——, Y.-H. Kim, S. Borchert, and U. Achatz, 2021: Toward transient subgrid-scale gravity wave representation in atmospheric models. Part I: Propagation model including nondissipative direct wave–mean-flow interactions. *J. Atmos. Sci.*, **78**, 1317–1338, https://doi.org/10.1175/JAS-D-20-0065.1.

Bretherton, F. P., 1966: The propagation of groups of internal gravity waves in a shear flow. *Quart. J. Roy. Meteor. Soc.*, **92**, 466–480, https://doi.org/10.1002/qj.49709239403.

Bronshtein, I. N., K. A. Semendyayev, G. Musiol, and H. Mühlig, 1990: *Handbook of Mathematics.* 5th ed. Springer-Verlag, 1164 pp.

Dunkerton, T. J., 1989: Theory of internal gravity wave saturation. *Pure Appl. Geophys.*, **130**, 373–397, https://doi.org/10.1007/BF00874465.

Eckermann, S. D., 2011: Explicitly stochastic parameterization of nonorographic gravity wave drag. *J. Atmos. Sci.*, **68**, 1749–1765, https://doi.org/10.1175/2011JAS3684.1.

Ertel, H., J.-J. Jaw, and S.-Z. Li, 1941: Tensorielle Theorie der Stabilität. *Meteor. Z.*, **58**, 389–392.

Falk, G., F. Herrmann, and G. B. Schmid, 1983: Energy forms or energy carriers? *Amer. J. Phys.*, **51**, 1074–1077, https://doi.org/10.1119/1.13340.

Fleming, E. L., S. Chandra, J. J. Barnett, and M. Corney, 1990: Zonal mean temperature, pressure, zonal wind and geopotential height as functions of latitude. *Adv. Space Res.*, **10**, 11–59, https://doi.org/10.1016/0273-1177(90)90386-E.

Fritts, D. C., 1989: A review of gravity wave saturation processes, effects, and variability in the middle atmosphere. *Pure Appl. Geophys.*, **130**, 343–371, https://doi.org/10.1007/BF00874464.

——, and M. J. Alexander, 2003: Gravity wave dynamics and effects in the middle atmosphere. *Rev. Geophys.*, **41**, 1003, https://doi.org/10.1029/2001RG000106.

Gardner, C. S., 1996: Testing theories of atmospheric gravity wave saturation and dissipation. *J. Atmos. Terr. Phys.*, **58**, 1575–1589, https://doi.org/10.1016/0021-9169(96)00027-X.

Gassmann, A., 2018: Entropy production due to subgrid-scale thermal fluxes with application to breaking gravity waves. *Quart. J. Roy. Meteor. Soc.*, **144**, 499–510, https://doi.org/10.1002/qj.3221.

——, and H.-J. Herzog, 2015: How is local material entropy production represented in a numerical model? *Quart. J. Roy. Meteor. Soc.*, **141**, 854–869, https://doi.org/10.1002/qj.2404.

Godson, W. L., 1950: Generalized criteria for dynamic instability. *J. Atmos. Sci.*, **7**, 268–278, https://doi.org/10.1175/1520-0469(1950)007<0268:GCFDI>2.0.CO;2.

Hasha, A., O. Bühler, and J. Scinocca, 2008: Gravity wave refraction by three-dimensional varying winds and the global transport of angular momentum. *J. Atmos. Sci.*, **65**, 2892–2906, https://doi.org/10.1175/2007JAS2561.1.

Hauf, T., and H. Höller, 1987: Entropy and potential temperature. *J. Atmos. Sci.*, **44**, 2887–2901, https://doi.org/10.1175/1520-0469(1987)044<2887:EAPT>2.0.CO;2.

Henyey, F. S., 1986: Strange semiclassical phenomena for the equation $\nabla^2\partial_t^2\phi + a(\partial_x^2 + \partial_y^2)\phi + b\partial_\phi^2 = 0$, describing waves in stratified fluids. *The Physics of Phase Space: Nonlinear Dynamics and Chaos, Geometric Quantization, and Wigner Function*, Y. S. Kim and W. W. Zachary, Eds., Vol. 278, Springer, 322–327, https://doi.org/10.1007/3-540-17894-5_374.

——, and N. Pomphrey, 1983: Eikonal description of internal wave interactions: A non-diffusive picture of "induced diffusion." *Dyn. Atmos. Oceans*, **7**, 189–219, https://doi.org/10.1016/0377-0265(83)90005-2.

Herbert, F., 1978: The tensor structure of constitutive equations for linear atmospheric heat and momentum exchange with axisymmetric coefficients. Deutscher Wetterdienst Rep. 145, 42 pp.

——, and F. Kucharski, 1998: An internal energy theorem for the atmosphere and its association with turbulent (potential) temperature variances. *Geophys. Res. Lett.*, **25**, 1185–1188, https://doi.org/10.1029/98GL00914.

Hertzog, A., C. Souprayen, and A. Hauchecorne, 2002: Eikonal simulations for the formation and the maintenance of atmospheric gravity wave spectra. *J. Geophys. Res.*, **107**, 4145, https://doi.org/10.1029/2001JD000815.

Hines, C. O., 1971: Generalizations of the Richardson criterion for the onset of atmospheric turbulence. *Quart. J. Roy. Meteor. Soc.*, **97**, 429–439, https://doi.org/10.1002/qj.49709741405.

——, 1988: Generation of turbulence by atmospheric gravity waves. *J. Atmos. Sci.*, **45**, 1269–1278, https://doi.org/10.1175/1520-0469(1988)045<1269:GOTBAG>2.0.CO;2.

——, 1997: Doppler-spread parameterization of gravity-waves momentum deposition in the middle atmosphere. Part 1: Basic formulation. *J. Atmos. Sol.-Terr. Phys.*, **59**, 371–386, https://doi.org/10.1016/S1364-6826(96)00079-X.

Hodges, R. R., Jr., 1967: Generation of turbulence in the upper atmosphere by internal gravity waves. *J. Geophys. Res.*, **72**, 3455–3458, https://doi.org/10.1029/JZ072i013p03455.

Holton, J. R., 2004: *An Introduction to Dynamic Meteorology*. 4th ed. Elsevier, 553 pp.

Job, G., and F. Herrmann, 2006: Chemical potential—A quantity in search of recognition. *Eur. J. Phys.*, **27**, 353–371, https://doi.org/10.1088/0143-0807/27/2/018.

Jones, W. L., 1969: Ray tracing for internal gravity waves. *J. Geophys. Res.*, **74**, 2028–2033, https://doi.org/10.1029/JB074i008p02028.

——, 1971: Energy-momentum tensor for linearized waves in material media. *Rev. Geophys.*, **9**, 917–952, https://doi.org/10.1029/RG009i004p00917.

Jou, D., J. Casas-Vázquez, and G. Lebon, 2001: *Extended Irreversible Thermodynamics*. 3rd ed. Springer-Verlag, 463 pp.

Kim, Y.-H., G. Bölöni, S. Borchert, H.-Y. Chun, and U. Achatz, 2021: Toward transient subgrid-scale gravity wave representation in atmospheric models. Part II: Wave intermittency simulated with convective sources. *J. Atmos. Sci.*, **78**, 1339–1357, https://doi.org/10.1175/JAS-D-20-0066.1.

Kim, Y.-J., S. D. Eckermann, and H.-Y. Chun, 2003: An overview of the past, present and future of gravity-wave drag parametrization for numerical climate and weather prediction models. *Atmos.–Ocean*, **41**, 65–98, https://doi.org/10.3137/ao.410105.

Lebedev, L. P., M. J. Cloud, and V. A. Eremeyev, 2010: *Tensor Analysis with Applications in Mechanics*. 2nd ed. World Scientific Publishing, 380 pp.

Lindzen, R. S., 1981: Turbulence and stress owing to gravity wave and tidal breakdown. *J. Geophys. Res.*, **86**, 9707–9714, https://doi.org/10.1029/JC086iC10p09707.

Liu, Y., C. Liu, and D. Wang, 2011: Understanding atmospheric behaviour in terms of entropy: A review of applications of the second law of thermodynamics to meteorology. *Entropy*, **13**, 211–240, https://doi.org/10.3390/e13010211.

Majdzadeh, M., and G. P. Klaassen, 2019: An analysis of the Hines and Warner–McIntyre–Scinocca non-orographic gravity wave drag parametrizations. *Quart. J. Roy. Meteor. Soc.*, **145**, 2308–2334, https://doi.org/10.1002/qj.3559.

Marks, C. J., and S. D. Eckermann, 1995: A three-dimensional nonhydrostatic ray-tracing model for gravity waves: Formulation and preliminary results for the middle atmosphere. *J. Atmos. Sci.*, **52**, 1959–1984, https://doi.org/10.1175/1520-0469(1995)052<1959:ATDNRT>2.0.CO;2.

McLandress, C., 1998: On the importance of gravity waves in the middle atmosphere and their parameterization in general circulation models. *J. Atmos. Sol.-Terr. Phys.*, **60**, 1357–1383, https://doi.org/10.1016/S1364-6826(98)00061-3.

——, and J. F. Scinocca, 2005: The GCM response to current parameterizations of nonorographic gravity wave drag. *J. Atmos. Sci.*, **62**, 2394–2413, https://doi.org/10.1175/JAS3483.1.

Medvedev, A. S., and G. P. Klaassen, 2003: Thermal effects of saturating gravity waves in the atmosphere. *J. Geophys. Res.*, **108**, 4040, https://doi.org/10.1029/2002JD002504.

——, and E. Yiğit, 2019: Gravity waves in planetary atmospheres: Their effects and parameterization in global circulation models. *Atmosphere*, **10**, 531, https://doi.org/10.3390/atmos10090531.

Meixner, J., 1960: Die Thermodynamik irreversibler Prozesse. *Phys. Blätter*, **16**, 506–511, https://doi.org/10.1002/phbl.19600161003.

Muraschko, J., M. D. Fruman, U. Achatz, S. Hickel, and Y. Toledo, 2015: On the application of the Wentzel–Kramer–Brillouin theory for the simulation of the weakly nonlinear dynamics of gravity waves. *Quart. J. Roy. Meteor. Soc.*, **141**, 676–697, https://doi.org/10.1002/qj.2381.

Olbers, D., and C. Eden, 2013: A global model for the diapycnal diffusivity induced by internal gravity waves. *J. Phys. Oceanogr.*, **43**, 1759–1779, https://doi.org/10.1175/JPO-D-12-0207.1.

Onsager, L., 1931: Reciprocal relations in irreversible processes. I. *Phys. Rev.*, **37**, 405–426, https://doi.org/10.1103/PhysRev.37.405.

Papenfuß, C., 2020: *Continuum Thermodynamics and Constitutive Theory*. 1st ed. Springer, 238 pp.

Peixoto, J. P., A. H. Oort, M. D. Almeida, and A. Tomé, 1991: Entropy budget of the atmosphere. *J. Geophys. Res.*, **96**, 10 981–10 988, https://doi.org/10.1029/91JD00721.

Plougonven, R., A. de la Cámara, A. Hertzog, and F. Lott, 2020: How does knowledge of atmospheric gravity waves guide their parameterizations? *Quart. J. Roy. Meteor. Soc.*, **146**, 1529–1543, https://doi.org/10.1002/qj.3732.

Schlutow, M., 2019: Modulational stability of nonlinear saturated gravity waves. *J. Atmos. Sci.*, **76**, 3327–3336, https://doi.org/10.1175/JAS-D-19-0065.1.

Scinocca, J. F., 2003: An accurate spectral nonorographic gravity wave drag parameterization for general circulation models. *J. Atmos. Sci.*, **60**, 667–682, https://doi.org/10.1175/1520-0469(2003)060<0667:AASNGW>2.0.CO;2.

Shaw, T. A., and T. G. Shepherd, 2009: A theoretical framework for energy and momentum consistency in subgrid-scale parameterization for climate models. *J. Atmos. Sci.*, **66**, 3095–3114, https://doi.org/10.1175/2009JAS3051.1.

Shutts, G. J., and M. J. P. Cullen, 1987: Parcel stability and its relation to semigeostrophic theory. *J. Atmos. Sci.*, **44**, 1318–1330, https://doi.org/10.1175/1520-0469(1987)044<1318:PSAIRT>2.0.CO;2.

Sievers, U., 1984: The turbulent atmosphere and the inclusive system of model equations. *Beitr. Phys. Atmos.*, **57**, 324–345.

Sihvola, A., 1999: *Electromagnetic Mixing Formulas and Applications*. Institution of Engineering and Technology, 296 pp.

Snively, J. B., and V. P. Pasko, 2008: Excitation of ducted gravity waves in the lower thermosphere by tropospheric sources. *J. Geophys. Res.*, **113**, A06303, https://doi.org/10.1029/2007JA012693.

Song, I.-S., and H.-Y. Chun, 2008: A Lagrangian spectral parameterization of gravity wave drag induced by cumulus convection. *J. Atmos. Sci.*, **65**, 1204–1224, https://doi.org/10.1175/2007JAS2369.1.

——, C. Lee, H.-Y. Chun, J.-H. Kim, G. Jee, B.-G. Song, and J. T. Bacmeister, 2020: Propagation of gravity waves and its effects on pseudomomentum flux in a sudden stratospheric warming event. *Atmos. Chem. Phys.*, **20**, 7617–7644, https://doi.org/10.5194/acp-20-7617-2020.

Sonmor, L. J., and G. P. Klaassen, 1997: Toward a unified theory of gravity wave stability. *J. Atmos. Sci.*, **54**, 2655–2680, https://doi.org/10.1175/1520-0469(1997)054<2655:TAUTOG>2.0.CO;2.

Souprayen, C., J. Vanneste, and A. H. A. Hauchecorne, 2001: Atmospheric gravity wave spectra: A stochastic approach.

J. Geophys. Res., **106**, 24 071–24 086, https://doi.org/10.1029/2001JD900043.

Stephan, C. C., H. Schmidt, C. Zülicke, and V. Matthias, 2020: Oblique gravity wave propagation during sudden stratospheric warmings. *J. Geophys. Res. Atmos.*, **125**, e2019JD031528, https://doi.org/10.1029/2019JD031528.

Strube, C., P. Preusse, M. Ern, and M. Riese, 2021: Propagation paths and source distributions of resolved gravity waves in ECMWF-IFS analysis fields around the southern polar night jet. *Atmos. Chem. Phys.*, **21**, 18 641–18 668, https://doi.org/10.5194/acp-21-18641-2021.

Viúdez, A., 2005: The vorticity–velocity gradient cofactor tensor and the material invariant of the semigeostrophic theory. *J. Atmos. Sci.*, **62**, 2294–2301, https://doi.org/10.1175/JAS3482.1.

Walters, D., and Coauthors, 2019: The Met Office Unified Model Global Atmosphere 7.0/7.1 and JULES Global Land 7.0 configurations. *Geosci. Model Dev.*, **12**, 1909–1963, https://doi.org/10.5194/gmd-12-1909-2019.

Warner, C. D., and M. E. McIntyre, 2001: An ultrasimple spectral parameterization for nonorographic gravity waves. *J. Atmos. Sci.*, **58**, 1837–1857, https://doi.org/10.1175/1520-0469(2001)058<1837:AUSPFN>2.0.CO;2.

Wei, J., G. Bölöni, and U. Achatz, 2019: Efficient modeling of the interaction of mesoscale gravity waves with unbalanced large-scale flows: Pseudomomentum-flux convergence versus direct approach. *J. Atmos. Sci.*, **76**, 2715–2738, https://doi.org/10.1175/JAS-D-18-0337.1.

Wilson, E. B., 1929: *Vector Analysis: A Text-Book for the Use of Students of Mathematics and Physics, Founded upon the Lectures of J. Willard Gibbs*. Yale University Press, 480 pp.

Zdunkowski, W., and A. Bott, 2003: *Dynamics of the Atmosphere: A Course in Theoretical Meteorology*. Cambridge University Press, 738 pp.

——, and ——, 2004: *Thermodynamics of the Atmosphere: A Course in Theoretical Meteorology*. Cambridge University Press, 251 pp.